SINC, a type III secreted protein of *Chlamydia psittaci*, targets the inner nuclear membrane of infected cells and uninfected neighbors

Sergio A. Mojica[a], Kelley M. Hovis[a], Matthew B. Frieman[b], Bao Tran[c], Ru-ching Hsia[d], Jacques Ravel[b,e], Clifton Jenkins-Houk[f], Katherine L. Wilson[f], and Patrik M. Bavoil[a]

[a]Department of Microbial Pathogenesis and [d]Core Imaging Facility and Department of Neural and Pain Sciences, University of Maryland School of Dentistry, Baltimore, MD 21201; [b]Department of Microbiology and Immunology and [e]Institute for Genome Science, University of Maryland School of Medicine, Baltimore, MD 20201; [c]Mass Spectrometry Center, University of Maryland School of Pharmacy, Baltimore, MD 21201; [f]Department of Cell Biology, Johns Hopkins University School of Medicine, Baltimore, MD 21205

ABSTRACT **SINC, a new type III secreted protein of the avian and human pathogen *Chlamydia psittaci*, uniquely targets the nuclear envelope of *C. psittaci*–infected cells and uninfected neighboring cells. Digitonin-permeabilization studies of SINC-GFP–transfected HeLa cells indicate that SINC targets the inner nuclear membrane. SINC localization at the nuclear envelope was blocked by importazole, confirming SINC import into the nucleus. Candidate partners were identified by proximity to biotin ligase-fused SINC in HEK293 cells and mass spectrometry (BioID). This strategy identified 22 candidates with high confidence, including the nucleoporin ELYS, lamin B1, and four proteins (emerin, MAN1, LAP1, and LBR) of the inner nuclear membrane, suggesting that SINC interacts with host proteins that control nuclear structure, signaling, chromatin organization, and gene silencing. GFP-SINC association with the native LEM-domain protein emerin, a conserved component of nuclear "lamina" structure, or with a complex containing emerin was confirmed by GFP pull down. Our findings identify SINC as a novel bacterial protein that targets the nuclear envelope with the capability of globally altering nuclear envelope functions in the infected host cell and neighboring uninfected cells. These properties may contribute to the aggressive virulence of *C. psittaci*.**

Monitoring Editor
Robert D. Goldman
Northwestern University

Received: Nov 12, 2014
Revised: Mar 2, 2015
Accepted: Mar 6, 2015

INTRODUCTION

Members of the genus *Chlamydia* are ubiquitous Gram-negative bacteria capable of infecting a wide variety of hosts and tissues (Corsaro and Venditti, 2004). Among 11 recognized species, 2—*Chlamydia trachomatis* and *Chlamydia pneumoniae*—commonly infect humans and pose significant public health challenges. *C. trachomatis*, a genital and ocular pathogen, is the most common bacterial infection in the United States, with an estimated 2.8 million infections annually (Satterwhite *et al.*, 2011). *C. pneumoniae*, a clinically significant respiratory pathogen, causes atypical pneumonia and has been implicated in cardiovascular disease (Kuo *et al.*, 1995). Most primary infections with *C. trachomatis* are strictly limited to the mucosal epithelium of two human anatomical sites, the conjunctiva and genital tract, where symptoms may be mild to nonexistent. However, chronic *C. trachomatis* infection leads to inflammatory damage with potentially severe sequelae, including blindness, pelvic inflammatory disease, ectopic pregnancy, and infertility (Stamm, 1999). Two other species, *Chlamydia psittaci* and *Chlamydia abortus*, can be transmitted from animals to humans (zoonotic infection) and cause severe disease (Rohde *et al.*, 2010). *C. psittaci* is widespread—detected in nearly 500 avian species (Kaleta and Taday, 2003)—in which infection can be either latent or systemic with clinically overt respiratory symptoms (Stewardson and Grayson, 2010). *C. psittaci* is a highly infectious, medically significant potential human pathogen classified as a category B bioterrorism agent by

This article was published online ahead of print in MBoC in Press (http://www.molbiolcell.org/cgi/doi/10.1091/mbc.E14-11-1530) on March 18, 2015.

Address correspondence to: Patrik M. Bavoil (pbavoil@umaryland.edu).

Abbreviations used: EB, elementary body; IEM, immuno–electron microscopy; INM, inner nuclear membrane; MOMP, major outer membrane protein; NE, nuclear envelope; RB, reticulate body; SINC, secreted inner nuclear membrane–associated *Chlamydia* protein; T3S, type III secretion.

the Centers for Disease Control and Prevention (www.bt.cdc.gov/agent/agentlist-category.asp). Inhalation via aerosols can cause life-threatening pneumonia (Smith *et al.*, 2011) and systemic complications, including encephalitis and endocarditis (Salisch *et al.*, 1996). Infection can be unapparent (asymptomatic) or manifest with high fever, difficulty breathing, and nonproductive cough, low pulse, chills, headache, and myalgia and is potentially fatal in untreated patients (Moroney *et al.*, 1998). Exposure is typically due to contact with reservoirs of zoonotic psittacosis (poultry, pet parrots, free-living pigeons) or outdoor activities (e.g., lawn mowing or gardening) presumably associated with inhalation of bird fecal dust (Beeckman and Vanrompay, 2009). Person-to-person transmission of psittacosis is possible but rare (Ito *et al.*, 2002). The mechanisms that allow *C. psittaci* to be significantly more infectious and pathogenic than *C. trachomatis* in humans are not understood.

All *Chlamydia* species are obligate intracellular pathogens with a unique developmental life cycle involving two cellular forms. After entering the host cell via endocytosis, metabolically dormant chlamydiae—termed elementary bodies (EBs)—differentiate into larger, actively replicating reticulate bodies (RBs) within a membrane-bound vacuole termed the inclusion. RBs differentiate back into EBs asynchronously, so the chlamydial inclusion includes both forms (RBs and EBs) at late stages of infection. After completing development, EBs exit upon lysis of the host cell or nonexocytic extrusion of whole or part of the inclusion (Hybiske and Stephens, 2007) and then either disseminate or infect neighboring cells.

All *Chlamydia* species encode a complete type III secretion (T3S) system that enables the direct translocation of effector proteins across both the bacterial envelope and host plasma membrane–derived inclusion membrane into the host cytosol, where they target specific host proteins and pathways to promote and maintain infection (Peters *et al.*, 2007). After a signal proposed to involve disruption of T3S "injectisome"-mediated RB contact with the inclusion membrane (Wilson *et al.*, 2006, 2009), RBs differentiate back into infectious EBs. The endoplasmic reticulum (ER) is closely apposed to the *C. trachomatis* inclusion surface (Derre *et al.*, 2011; Dumoux *et al.*, 2012), with at least one type III secreted inclusion membrane protein, IncA, colocalizing with ER markers (Giles and Wyrick, 2008). IncA is also involved in the fusion of small nascent vacuoles to form a single large inclusion (Suchland *et al.*, 2000; Delevoye *et al.*, 2004). The Inc family of T3S effectors includes many other, uncharacterized members (Bannantine *et al.*, 2000; Li *et al.*, 2008). Other well-characterized effectors include translocated actin recruitment protein (TARP; Clifton *et al.*, 2004) and CT694 (Hower *et al.*, 2009), both of which facilitate internalization by the host cell. Both are expressed late in development and are secreted early, suggesting potential "preloading" into the T3S injectisome during the RB-to-EB transition. TARP nucleates actin polymerization and is secreted within minutes of EB internalization (Clifton *et al.*, 2004). CT694 interacts with AHNAK and is believed to influence actin polymerization or membrane-associated signaling (Hower *et al.*, 2009). The late-expressed effector CopN is proposed to sense host cell contact, similar to *Yersinia* YopN (Fields and Hackstadt, 2000), but also modulates the host cytoskeleton (Archuleta *et al.*, 2011). Another effector, NUE, enters the nucleus and can methylate histones (Pennini *et al.*, 2010). Other putative effectors have been partially characterized (Hobolt-Pedersen *et al.*, 2009; Gong *et al.*, 2011; Muschiol *et al.*, 2011).

Although genetic methodologies are emerging for *Chlamydia* (Wang *et al.*, 2011), the major obstacle to identifying and characterizing T3S-dependent chlamydial effectors has been the combined effect of the genetic intractability of *Chlamydia* and the impracticality of clonal isolation. Strategies that have been successful include identification based on homology to effectors from other bacterial genera (Hsia *et al.*, 1997), affinity to T3S chaperones (Fields *et al.*, 2005), subcellular fractionation (Hobolt-Pedersen *et al.*, 2009) of *Chlamydia*-infected cells, and heterologous secretion assays in *Yersinia*, *Shigella*, and *Salmonella* (Fields and Hackstadt, 2000; Subtil *et al.*, 2001, 2005; Ho and Starnbach, 2005; Hower *et al.*, 2009; Hovis *et al.*, 2013; da Cunha *et al.*, 2014). We previously used the T3S system of *Yersinia pseudotuberculosis* as a surrogate to test putative chlamydial T3S-dependent secreted proteins predicted by the protein homology-based algorithm SIEVE (Samudrala *et al.*, 2009). This strategy identified the hypothetical product of *orf70* (NCBI G5Q_0070) of *C. psittaci* strain CAL10 as a putative effector (Hovis *et al.*, 2013). We report here the characterization of this protein, renamed secreted inner nuclear membrane–associated *Chlamydia* protein (SINC), based on its novel localization at the nuclear envelope (NE) of infected and neighboring uninfected cells and association with nuclear membrane proteins.

RESULTS

sinC is syntenic and encodes a weak orthologue of *C. trachomatis* CT694

The *C. psittaci* putative effector gene *sinC* was chosen for further investigation because it posed a paradox: *sinC* is syntenic with *ct694* of *C. trachomatis*, each downstream of the phosphoglycerate kinase gene, *pgk* (Supplemental Figure S1A); however, the encoded CT694 and SINC proteins are only 12.5% identical, compared with 74% identical phosphoglycerate kinase proteins. Residual identity to CT694 is scattered throughout SINC (e.g., residues 1–11, 151–161, and 458–466), suggesting divergence from a common ancestral gene.

Low sequence identity suggested that SINC and CT694 were functionally distinct and might therefore be expressed at different stages of development in *C. psittaci*– or *C. trachomatis*–infected cells. Reverse transcription quantitative PCR (RT-qPCR) analysis of HeLa-grown *C. psittaci* CAL10 revealed low or background levels of *sinC* transcripts from 6 to 24 h postinfection (hpi), peaking at 30–42 hpi and decreasing sharply by 42 hpi, with a strong trend toward statistical significance ($H = 13.675$, $p = 0.057$; Supplemental Figure S1B), similar to *ct694*. We raised polyclonal SINC-specific antibodies (α-SINC; see *Materials and Methods*) that specifically recognized a 55-kDa protein in *C. psittaci*–infected HeLa cells starting at 30 hpi (Supplemental Figure S1B). Immunoblotting for SINC and the major outer membrane protein (MOMP) showed that SINC protein levels remained high at 48 hpi (Supplemental Figure S1B), suggesting that it is relatively stable. Because *sinC* and *ct694* and their gene products were expressed at similar times during development (Belland *et al.*, 2003; Hower *et al.*, 2009), we reasoned that they must differ in some other way.

SINC accumulates at the NE in infected cells and nearby noninfected cells

To locate SINC, infected HeLa cells were fixed with methanol, stained, and examined by indirect immunofluorescence either 24 (Figure 1) or 36 hpi (Figure 2). Consistent with immunoblot results, SINC was detected by indirect immunofluorescence staining at 24 hpi as dispersed punctate signals inside the chlamydiae-packed inclusions (Figure 1A); these 24-hpi signals often colocalized with the housekeeping protein elongation factor Tu (EF-Tu), suggesting localization within individual bacteria. SINC staining was unevenly distributed, with no apparent spatial position within the inclusion (e.g., lumen vs. periphery), consistent with asynchronous chlamydial

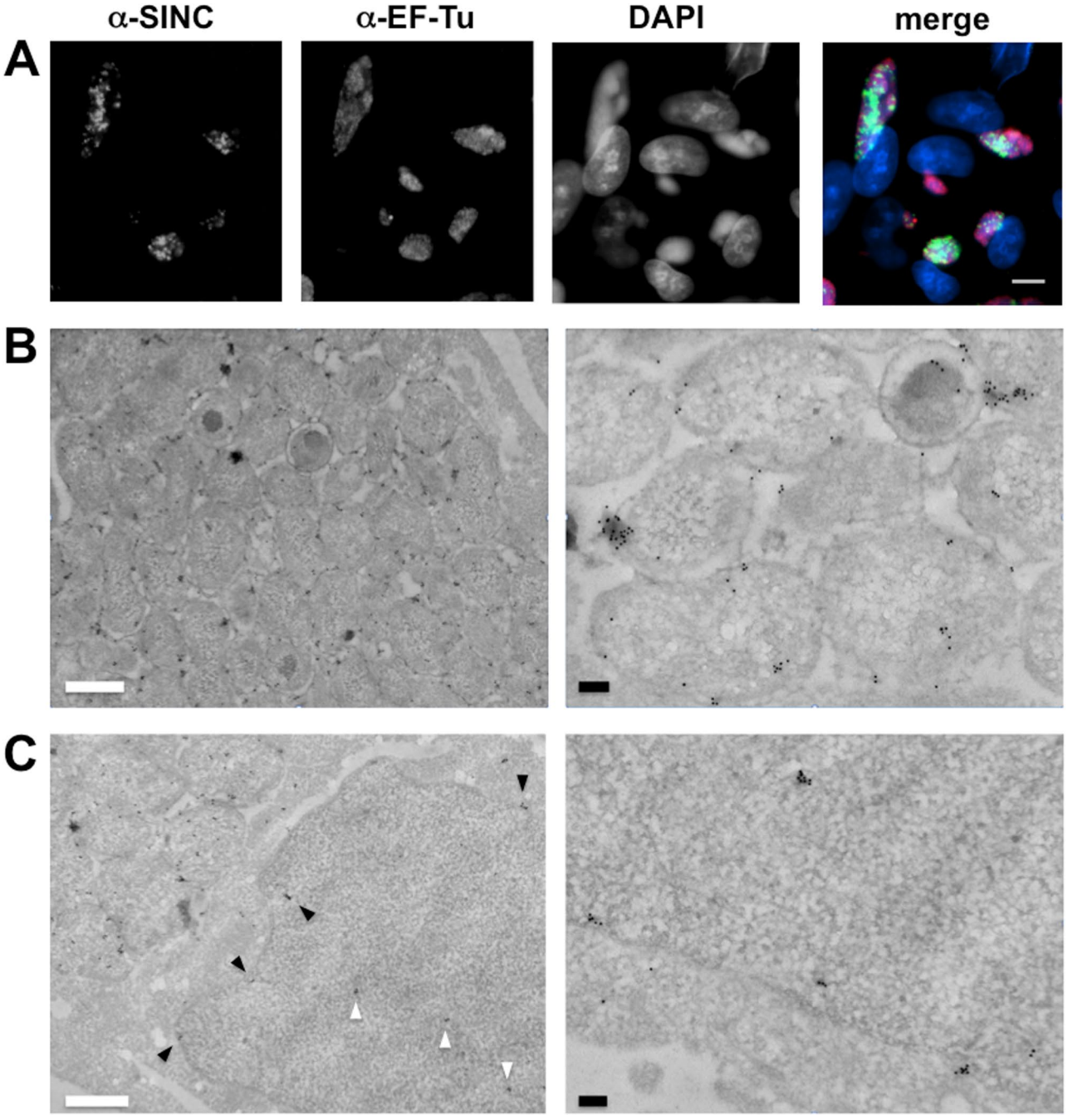

FIGURE 1: SINC is mostly associated with chlamydiae within the inclusion at mid to early-late development. (A) Immunofluorescence images of *C. psittaci* CAL10–infected HeLa cells fixed with methanol at 24 hpi and stained using antibodies specific for SINC (α-SINC) and for elongation factor Tu (α–EF-Tu). DNA was DAPI stained; epifluorescence images were obtained on a Zeiss Axio Imager Z.1 (40×objective). Bar, 10 μm. (B, C) IEM images of *C. psittaci* CAL10–infected HeLa cells fixed with PFA at 24 hpi using colloidal gold–conjugated antibodies specific for SINC (α-SINC). (C) Black and white arrowheads identify SINC signals at the NE and a putative nucleoplasmic "track" consistent with pore-linked filaments, respectively. Bars, 500 nm (white), 100 nm (black).

development. Immuno–electron microscopy (IEM) of 24-hpi cultures revealed SINC association with the cytoplasm and membranes of RBs and intermediate bodies (Figure 1B), with a disproportionate concentration of gold particles associated with the chlamydial surface, consistent with ongoing production and T3S. Moreover, SINC-specific gold particles were often arranged in pairs or triplets (e.g., Figure 1B), or as clusters associated with an electron-opaque mass extending from the chlamydial surface, suggesting that secreted SINC associates with a large, potentially polymeric structure. IEM of 24-hpi cultures also revealed a few SINC-gold pairs, triplets, and clusters at the NE and nucleoplasm (Figure 1C).

At 36 hpi, nearly all chlamydiae within the inclusion were SINC positive as visualized by confocal microscopy (Figure 2A). We also detected strong SINC-specific fluorescence at the host cell NE, especially on the side nearest the inclusion (Figure 2A) and weak SINC staining in the nucleoplasm (Figure 2B), consistent with IEM

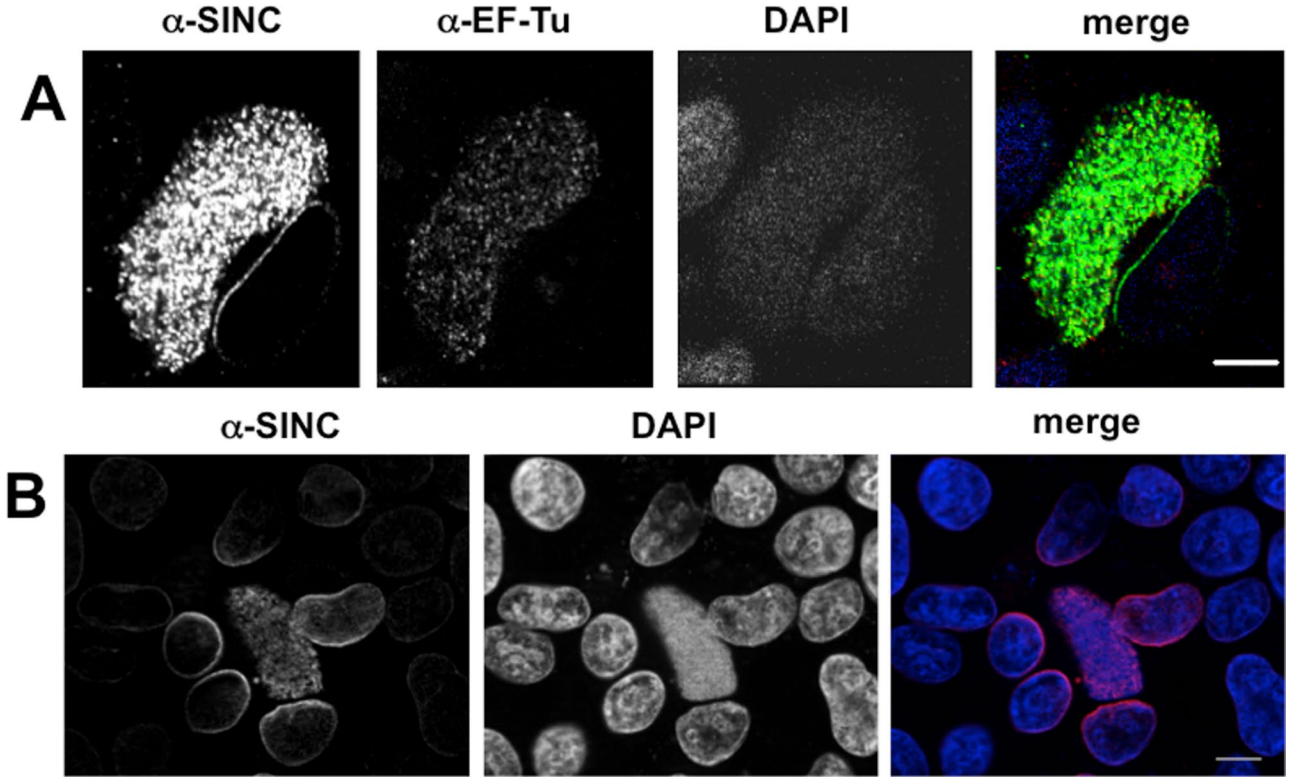

FIGURE 2: SINC is secreted by chlamydiae and targets the nuclear envelope of infected and uninfected neighboring cells late in development. Immunofluorescence images of *C. psittaci* CAL10–infected HeLa cells fixed with methanol at 36 hpi and stained using antibodies specific for SINC (α-SINC) and for elongation factor Tu (α–EF-Tu; A) or for SINC alone (B). DNA was stained with DAPI. (A) Confocal images (Zeiss LSM 510 Meta Confocal Microscope) indicate SINC signal at the NE. (B) Epifluorescence images (Zeiss Axio Imager Z.1 with ApoTome.2 module) indicate SINC signal at the NE of the infected cell and that of neighboring uninfected cells. Bars, 10 μm.

(Figure 1C). These and later images hinted that SINC might colocalize with pore-linked filaments extending into the nucleoplasm (e.g., white arrowheads in Figures 1C and 3A; Arlucea *et al.*, 1998; Fontoura *et al.*, 2001; Kiseleva *et al.*, 2004). To our surprise, SINC also localized prominently at the NE of neighboring uninfected cells, on the side of the nucleus facing the infected cell, akin to a "light bulb" shining on surrounding objects (Figure 2B). Owing to the low multiplicity of infection, most infected cells were surrounded by uninfected immediate neighbors, which, without exception, displayed this phenotype. Thus SINC had two novel characteristics: stable association with the NE of human cells—unprecedented for a bacterial protein—and translocation to neighboring cells—unprecedented for the genus *Chlamydia*.

SINC localization at the NE is sensitive to nuclear import inhibition

IEM (Figure 1, B and C) suggested that SINC enters the nucleus via NPCs. To test this idea, HeLa cells were infected and incubated for 24 h with dimethyl sulfoxide (DMSO) plus or minus 22.5 μM importazole, a specific importin β inhibitor (Soderholm *et al.*, 2011). Indirect immunofluorescence staining of DMSO-treated controls, imaged with or without an Apotome-2 module AT2 to eliminate stray light and enhance resolution, revealed SINC in bacterial inclusions and at the NE of both infected cells and uninfected neighbors, with weaker signals in the nucleoplasm (Figure 3A), as expected. By contrast, SINC was detected in the inclusion but was markedly reduced at the NE of importazole-treated cells (Imp, Imp/AT2, Figure 3A; quantified in Figure 3B). Inhibition was dose dependent (unpublished data) and peaked near the reported IC_{50} of importazole (25 μM; Figure 3B). We conclude that SINC is imported into the infected cell nucleus via the NPC. Because SINC has no predicted nuclear localization signal (NLS) or transmembrane domain, we favor models in which SINC entry requires an NLS-bearing partner. SINC showed no obvious accumulation elsewhere in importazole-treated infected cells and was not detected at the NE of uninfected neighbors, both consistent with its dispersal throughout the cytosol (or retention in chlamydiae) when nuclear import was blocked.

SINC–green fluorescent protein targets the NE in transfected HeLa cells and transformed yeast cells

SINC localization at the NE was independently validated in live and fixed HeLa cells by direct fluorescence 24 h after transfection with a plasmid encoding SINC–green fluorescent protein (GFP; Figure 4, A and B). SINC-GFP localized uniformly along the NE, as expected for an exogenous protein translated throughout the cytoplasm. GFP-fused SINC orthologues from two species, *C. abortus* (Thomson *et al.*, 2005) and *Chlamydia caviae* (Read *et al.*, 2003), also localized at the NE of transfected HeLa cells (Table 1, Supplemental Figure S2, and Figure 4C). The *C. trachomatis* control, CT694-GFP, distributed diffusely and concentrated near the plasma membrane (Figure 4C), as expected (Hower *et al.*, 2009; Bullock *et al.*, 2012). Predicted orthologous polypeptides from *Candidatus* Chlamydia ibidis (Vorimore *et al.*, 2013), *Chlamydia pecorum* (Mojica *et al.*, 2011), and *C. pneumoniae* (Read *et al.*, 2000), which have "mixed" homology (e.g., the *C. pecorum* orthologue is 17% identical to SINC and 19% identical to CT694) failed to localize at the NE in transfected

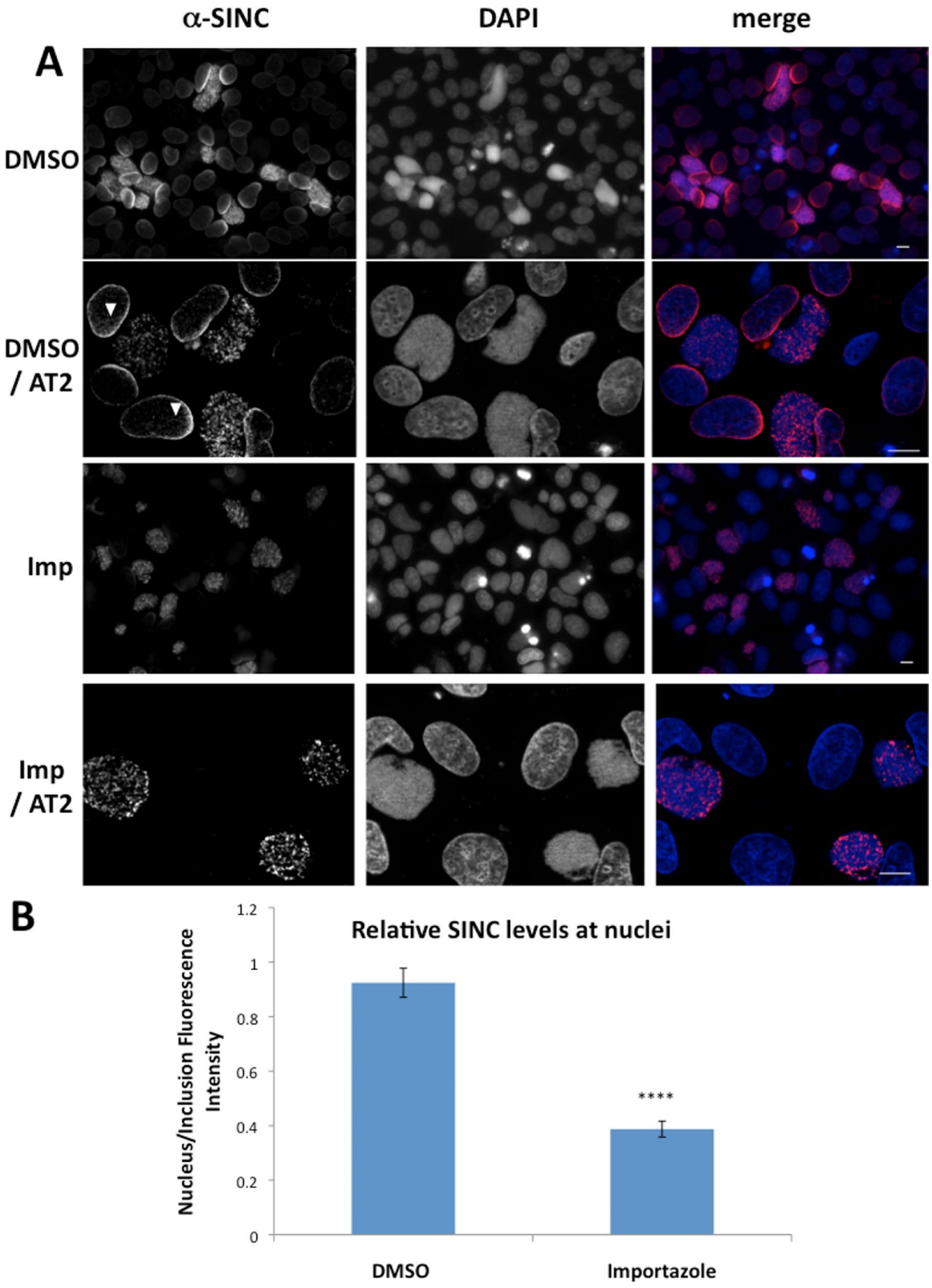

FIGURE 3: Nuclear import inhibitor importazole blocks SINC localization at the NE. (A) Indirect immunofluorescence images (Zeiss Axio Imager Z.1 fluorescence microscope without or with [AT2] the ApoTome.2 module) of *C. psittaci* CAL10–infected HeLa cells grown in the presence of either importazole (Imp, 22.5 μM) or DMSO starting at 24 hpi and then fixed at 36 hpi and stained with DAPI (blue) and antibodies specific for SINC (α-SINC; red). White arrowheads in DMSO/AT2 and α-SINC indicate thread-like nucleoplasmic signals consistent with pore-linked filaments. Bars, 10 μm. (B) SINC localization at the NE was quantified as the ratio of nucleus-specific to inclusion-specific fluorescence intensities (average of 20 cells) using the colocalization module of AxioVision software release 4.8. ****$p < 0.0001$.

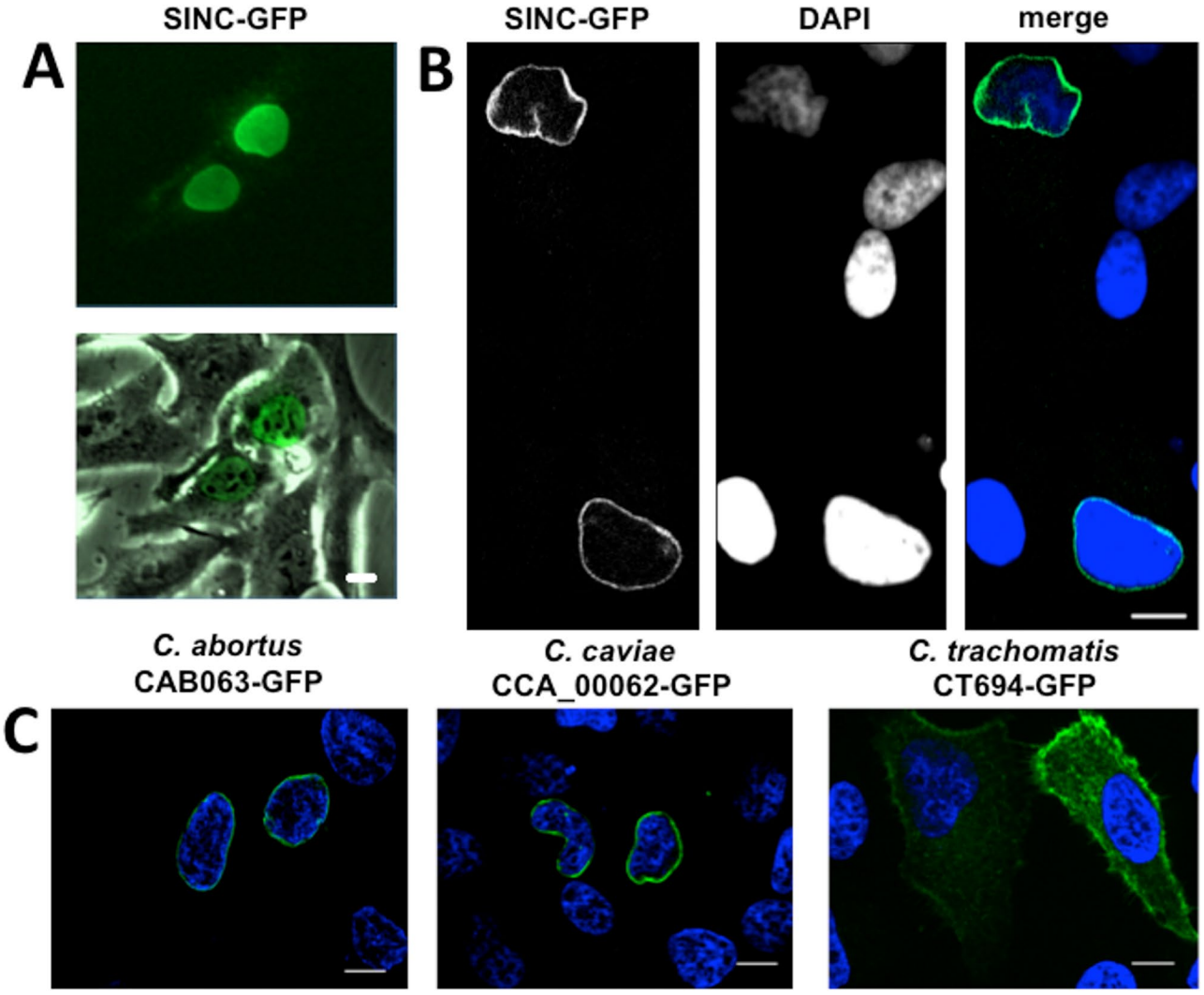

FIGURE 4: GFP-SINC and SINC orthologues from *C. abortus* and *C. caviae* each localize at the nuclear envelope of transfected cells. (A–C) Direct GFP fluorescence images of live (A) or methanol-fixed (B, C) HeLa cells at 24 h posttransfection with plasmids encoding GFP-fused SINC (pCAGGS-*sinC*-GFP), *C. abortus* CAB063-GFP (pCAGGS-*cab063*-GFP), *C. caviae* CCA_00062-GFP (pCAGGS-*cca062*-GFP), or *C. trachomatis* CT694 (pCAGGS-*ct694*-GFP). DNA was DAPI stained. (A) Epifluorescence (top) and epifluorescence plus phase images (Olympus IX81 microscope for Live Cell Imaging, Olympus America, Center Valley, PA). (B) Confocal images (Zeiss LSM 510 Meta Confocal Microscope). (C) Epifluorescence images (Zeiss Axio Imager Z.1 with the ApoTome.2 module). Bars, 10 μm.

cells (Table 1, and unpublished data). SINC orthologues in two recently described avian species, *Chlamydia avium* and *Chlamydia gallinacea* (Sachse *et al.*, 2014), and CT694 orthologues in *Chlamydia suis* and *Chlamydia muridarum* (Table 1), were not tested. Several other published *C. psittaci* genomes (Chu *et al.*, 2014) contain *C. avium* or *Cand.* C. ibidis–like SINC orthologues (unpublished data). These SINC-based relationships are consistent with phylogenetic relationships among the *Chlamydiaceae* (Horn *et al.*, 2004) and suggest that all *sinC* and *ct694* orthologues evolved from a common ancestral gene. SINC-GFP also localized at the NE in both live and paraformaldehyde-fixed transformed yeast (*Saccharomyces cerevisiae*) cells (Supplemental Figure S3, A and B, respectively). We concluded that the SINC polypeptide is sufficient to localize at the NE of eukaryotic cells; no other bacterial products were required.

By contrast, untagged SINC (expressed from pCAGGS-*sinC*; unpublished data) and SINC-GFP (expressed from pCAGGS-*sinC*-GFP; Figure 4) were each apparently insufficient to translocate from strongly expressing cells to neighboring cells: we detected little if any SINC or SINC-GFP signal at the NE of neighboring cells and saw no evidence of the characteristic "light bulb" effect, implying that additional chlamydial factor(s) were required for SINC transport to neighboring cells.

Sequence alignments of SINC, CAB063, and CCA_00062 revealed many conserved regions, including SINC residues 1–22 (presumed type III secretion signal) and ^{136}DSARSTEGAARGLQKKGY^{153}, ^{173}RPNTPPPPPPT^{183}, ^{219}KRKAPQPP^{226}, ^{268}KLKAELEA^{275}, ^{346}RSIWDLGEKEQRQDGESVLL^{368}, ^{425}NPNGMKKFWSSFAGKGE^{441}, and ^{469}RWNAGALDLM^{478} (Supplemental Figure S2). We concluded that SINC localization at the NE is a conserved feature of two known aggressive zoonotic pathogens: *C. psittaci* and *C. abortus*. Although *Chlamydia caviae* infection of guinea pigs is used extensively to model *C. trachomatis* oculogenital infection of humans (Rank, 1994; Rank and Whittum-Hudson, 1994), the zoonotic potential of this third SINC-expressing species, *C. caviae*, and the extent and severity

Chlamydia species	Strain	Open reading frame	Percentage identity[a]	Targets NE?
C. psittaci	CAL10	G5Q_0070	100	Yes
C. abortus	S26/3	CAB063	76	Yes
C. caviae	GPIC	CCA_00062	54	Yes
C. felis	Fe/C-56	CF0942	54	Not tested
C. avium	10DC88	M832_08640	32	Not tested
C. gallinacea	08-1274/3	M787_0805	30	Not tested
Cand. C. ibidis	10-1398/6	H359_0134	29	No
C. pneumoniae[b]	AR39	CP_0070	21.2	No
C. pecorum	E58	G5S_0369	17	No
C. suis	MD56	Q499_0753	14.6	Not tested
C. pneumoniae[b]	AR39	CP_0069	14.4	No
C. muridarum	MoPn Nigg	TC_0066	13.9	Not tested
C. trachomatis	D/UW-3Cx	CT694	12.5	No

[a]Percentage amino acid sequence identity to SINC (G5Q_0070).
[b]The SINC-orthologous sequence of *C. pneumoniae* corresponds to two open reading frames, CP_0069 and CP_0070.

TABLE 1: Percentage sequence identity and NE-tropism of SINC orthologues in the *Chlamydiaceae*.

of *C. caviae* infection in wild guinea pigs are all unknown (Lutz-Wohlgroth *et al.*, 2006). Despite its conservation in two clinically aggressive *Chlamydia* species, the SINC polypeptide revealed no mechanistic clues: we found no predicted hydrophobic or transmembrane domains, no predicted nuclear localization signal, and no predicted functional domains.

SINC targets the inner nuclear membrane

The NE is a complex structure (Wilson and Berk, 2010) with two membranes (inner and outer) that enclose a lumen contiguous with the ER and merge periodically to form holes ("pores") occupied by nuclear pore complexes (NPCs). NPCs control most molecular traffic into and out of the nucleus (Hatch and Hetzer, 2014). The NE and NPCs are supported and anchored by nuclear "lamina" structures, formed by three types of components: A- and B-type lamins (nuclear intermediate filaments), emerin and other LEM-domain proteins embedded in the inner nuclear membrane (INM), and their mutual partner, barrier to autointegration factor (BAF), a DNA/histone- and lamin-binding protein (Berk *et al.*, 2013b; Burke and Stewart, 2013). To determine whether SINC associated with the cytosolic, lumenal, or nucleoplasmic face(s) of the NE, we used digitonin, which selectively permeabilizes the plasma membrane but leaves NE membranes intact, thus blocking antibody access to epitopes in the lumen, INM, and nucleoplasm (Tissera *et al.*, 2010). Transfected HeLa cells expressing SINC-GFP for 24 h were fixed with paraformaldehyde (PFA) and permeabilized with either Triton X-100 (to solubilize all membranes) or digitonin. Cells were then double stained for SINC (Figure 5) plus either lamin A (Figure 5A) or tubulin (Figure 5B) as markers for the nuclear lamina and cytoplasm, respectively. SINC-GFP expression and NE localization were verified by direct GFP fluorescence (Figure 5, SINC-GFP). All three antibodies detected their epitopes in Triton X-100–permeabilized cells (Figure 5). However, only tubulin-specific antibodies (Figure 5B)—not lamin A- or SINC-specific antibodies (Figure 5A)—found their epitopes in digitonin-permeabilized cells. These results for exogenous SINC-GFP suggested that SINC specifically targets the INM/nuclear lamina. Another possibility—SINC localization within the NE lumen—was unlikely, given the "bacterium-to-cytosol" T3S mechanism, IEM localization results (Figure 1, B and C), and later results demonstrating SINC proximity to lamin B1 and other proteins outside the lumen.

Localization of GFP-fused SINC fragments

To characterize SINC functional domains involved in nuclear entry or NE targeting, we transfected HeLa cells with GFP-fused SINC fragments named A (SINC residues 1–164), B (151–341), and C (332–502) and two larger fragments named AB (1–341) and BC (151–502; Figure 6A). Although potential mislocalization (e.g., due to misfolding or overexpression) was not ruled out, no fragment reproduced the characteristic NE localization of full-length SINC-GFP. The B-GFP and C-GFP constructs localized diffusely throughout cells; B-GFP showed mild accumulation in the nucleoplasm (Figure 6B), and neither concentrated at the NE, suggesting that INM association required fragment A. A-GFP associated with ER/NE and potentially other organelle membranes but did not enter the nucleus (Figure 6B). Consistent with roles in NE membrane association (fragment A) and entry and retention within the nucleus (fragment B), the combined AB-GFP polypeptide localized at the NE and also tended to aggregate in the nucleoplasm (Figure 6B). Nuclear shape appeared to be disrupted by overexpression of several fragments, particularly AB-GFP (Figure 6B). We therefore used the Matlab hTCP program (Chen *et al.*, 2013) to compare nuclear circularity in cells that expressed either wild-type SINC-GFP or AB-GFP and found that AB-GFP nuclei were significantly less circular (Supplemental Figure S5A; $p < 0.001$; two-tailed *t* test). Nuclear shape abnormalities suggested perturbed nuclear lamina structure and implicated SINC residues 1–341 (AB) in binding to INM or nuclear lamina protein(s), with fragment C somehow required to "balance" this activity. The BC-GFP polypeptide concentrated in the nucleoplasm with little or no accumulation at the NE, suggesting that fragment A is required to bind INM/lamina proteins. These results did not rule out high-affinity partner(s) at the INM but appear to favor "high-avidity" models in which SINC nuclear entry and accumulation at the INM involves multiple domains located throughout the polypeptide.

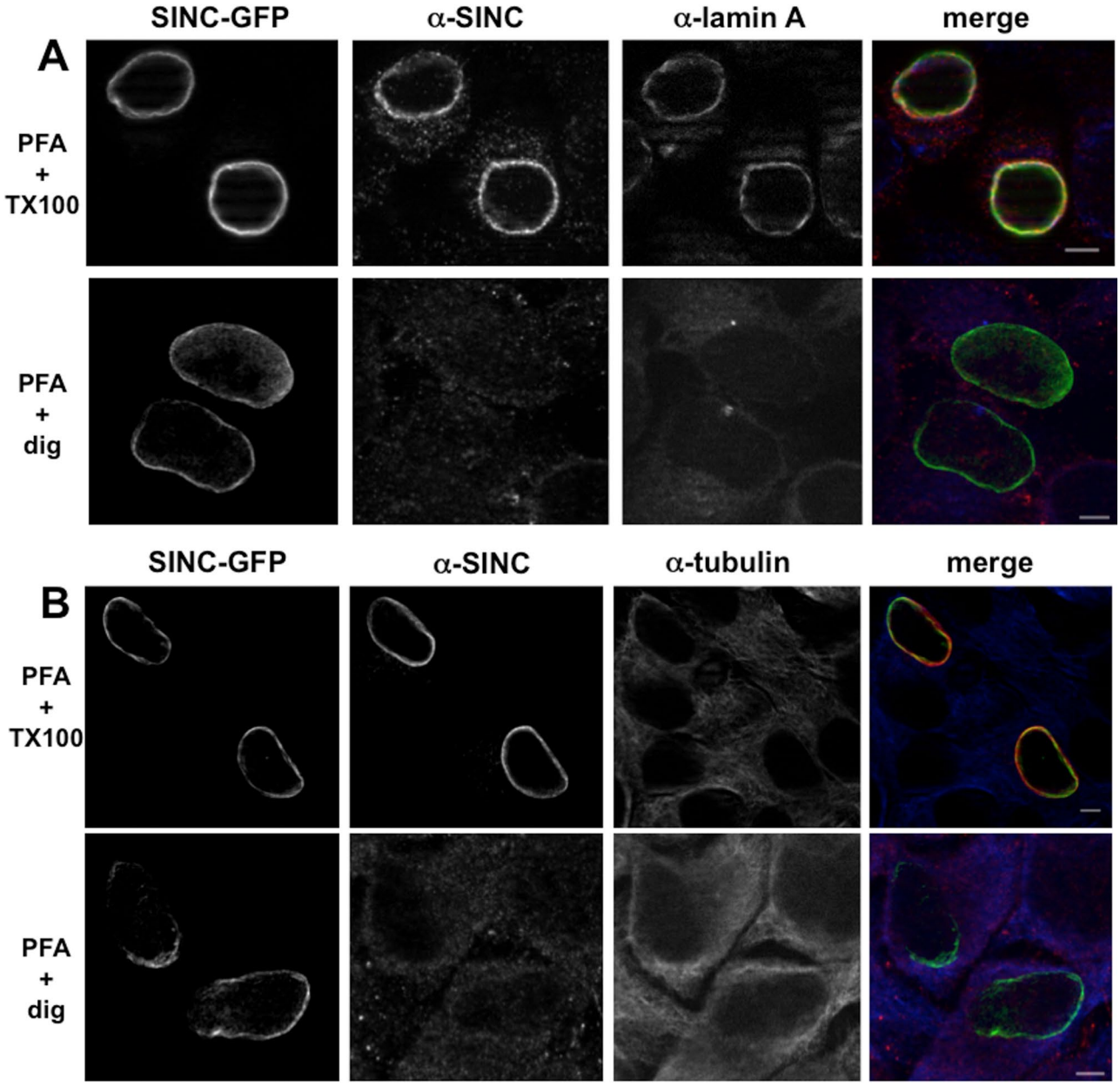

FIGURE 5: Digitonin- vs. Triton X-100 permeabilization of SINC-GFP–transfected cells. (A, B) At 24 h posttransfection, pCAGGS-*sinC*-GFP–transfected HeLa cells were fixed with PFA and treated with Triton X-100 (PFA + TX100) to permeabilize all membranes or fixed with PFA and treated with digitonin (PFA + dig) to permeabilize the plasma membrane only. Epifluorescence images (Zeiss Axio Imager Z.1 with the ApoTome.2 module) of cells double stained using antibodies specific for SINC (α-SINC) plus either lamin A (α-lamin A) or tubulin (α-tubulin) as markers of the nuclear lamina and cytoplasm, respectively. DNA was DAPI stained. Bars, 5 μm.

BioID identification of SINC-proximal human proteins

To understand the implications and mechanisms by which SINC targets the NE, we needed to identify potential host partner proteins. We used a new proximity-based in vivo biotinylation method, BioID, which successfully identified partners for lamin A (Roux *et al.*, 2012) and cell adhesion proteins ZO1 and E-cadherin (Van Itallie *et al.*, 2013, 2014). The crux of this method is that eukaryotic cells lack biotin; nearby proteins can be biotinylated by the biotin ligase (BirA) fusion only when cells are provided with external biotin (Roux *et al.*, 2012). Most identified ("proximal") proteins fall into two categories: direct partners, and associated proteins located within <10 nm—for example, in multiprotein complexes (Kim *et al.*, 2014). The negative control, myc-tagged BirA alone ("BirA-myc"), distributes throughout the cytoplasm and nucleoplasm and biotinylates many proteins nonspecifically (Roux *et al.*, 2012).

We transiently expressed either myc-tagged BirA (BirA-myc) or BirA-myc fused to the N-terminus of SINC (BirA-myc-SINC) in HeLa cells for 24 h. Indirect immunofluorescence staining with myc antibodies revealed BirA-myc throughout the cytoplasm and nucleus (unpublished results), as expected (Roux *et al.*, 2012), and verified that BirA-myc-SINC localized predominantly at the NE (Figure 7A). When cells were incubated plus or minus 50 μM biotin for 24 h

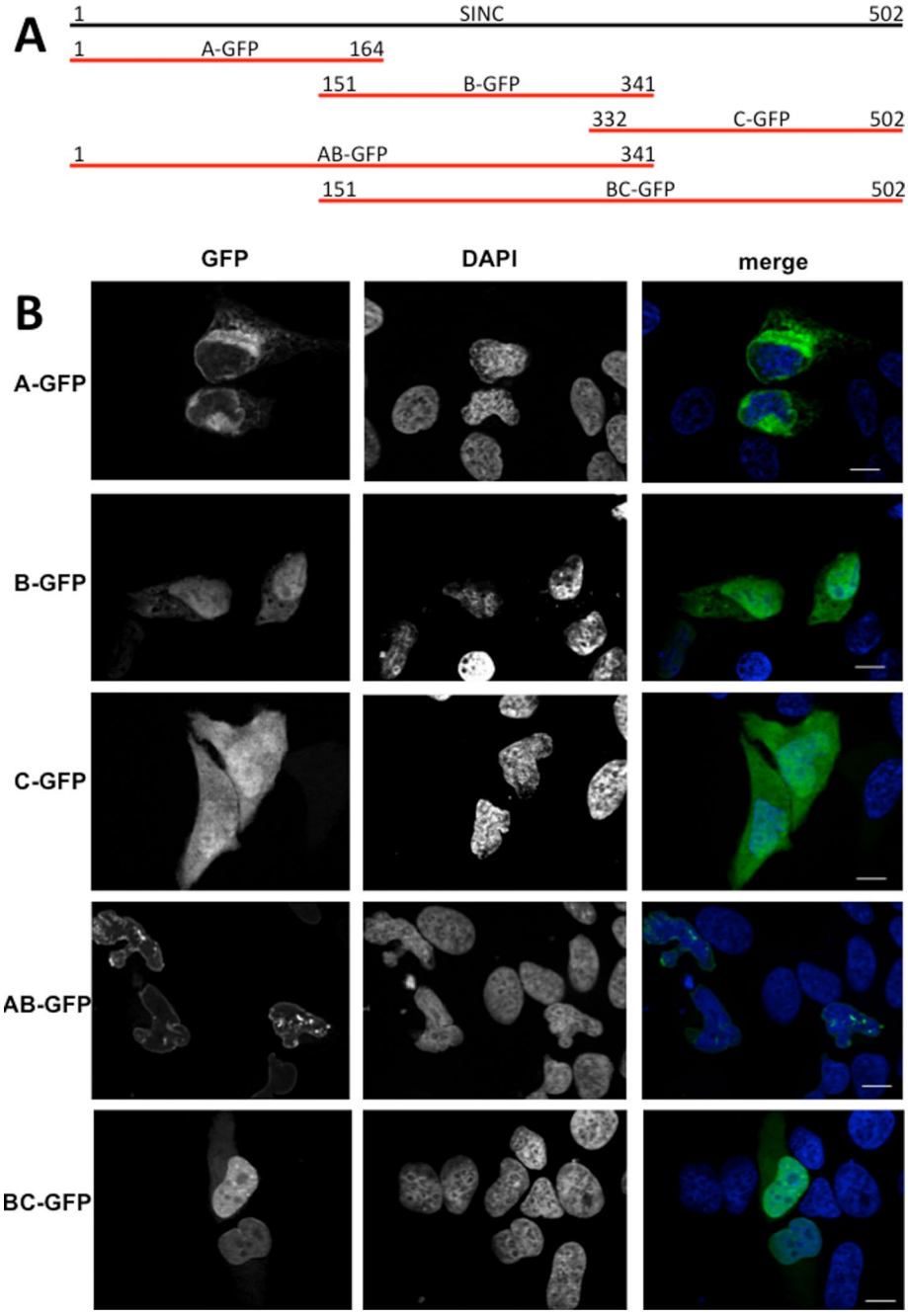

FIGURE 6: Subcellular localization of GFP-fused SINC fragments. (A) Schematic of the five tested SINC polypeptides, each fused at its C-terminus to GFP (not to scale). (B) Transfected HeLa cells expressing SINC-GFP fragments A, B, C, AB, and BC were fixed 24 h posttransfection, stained with DAPI, and imaged on a Zeiss Axio Imager Z.1 fluorescence microscope with the ApoTome.2 module. Bars, 10 μm.

before fixing and staining with fluorophore-conjugated streptavidin, we detected strong specific biotinylation of NE proteins in the presence, not absence, of biotin (Figure 7A).

To identify biotinylated SINC-proximal proteins, we used a more normal line of cells, namely human embryonic kidney (HEK293) cells, which stably expressed either BirA-myc or BirA-myc-SINC. Cells were cultured in medium supplemented with 50 μM biotin for 24 h. Biotinylated proteins were affinity purified from cell lysates using streptavidin beads; bound proteins were digested with trypsin, and released peptides were analyzed by mass spectrometry. Two independent experiments, BioID1 and BioID2, were performed. The BirA-myc controls identified many nonspecifically biotinylated proteins (288 in BioID1; 266 in BioID2; Figure 7B), consistent with the nonspecific distribution of BirA-myc throughout the cell. Fewer biotinylated proteins were identified in the BirA-myc-SINC samples (129 in BioID1; 146 in BioID2; Figure 7B), consistent with the major (NE) and minor (ER) subcellular locations of BirA-myc-SINC. BioID1 yielded 30 proteins unique to the BirA-myc-SINC data set; BioID2 identified 42 unique proteins, 22 of which were also identified in BioID1, for a total of 50 unique proteins (Figure 7C). The 22 proteins identified in both BioID experiments were deemed "high-confidence" candidates, likely to bind SINC directly or indirectly (e.g., via associated multiprotein complexes). Five of the six most abundantly recovered (based on spectral counts) proximal proteins reside at the INM—namely the LEM-domain proteins MAN1 and emerin, lamin B receptor (LBR), and lamina-associated polypeptide 1 (LAP1)—or the NE (ELYS, a NPC protein). The sixth was ABCD3, a peroxisomal membrane protein involved in long-chain fatty acid transport (Figure 7C). These results demonstrated SINC proximity to INM proteins with diverse roles in nuclear structure, signaling, and chromatin silencing at the NE (see *Discussion*).

Other high-confidence SINC-proximal proteins included lamin B1 and proteins with roles in nuclear import (importin α3), mRNA splicing (TADBP), ER structure and function (extended synaptotagmin, SRP receptor, UBXN4, CKAP4), vesicle traffic (synaptobrevin), innate immunity and signaling (MAVS, VRK2, AKAP1), and actin regulation (WASF2; Figure 7C). Two additional SINC-proximal proteins were identified in both BioID studies, based on having a ratio >3 for average spectral counts in BirA-myc-SINC versus BirA-myc samples: lamina- associated polypeptide 2 (LAP2; β/γ isoform[s]; LEM-domain protein[s] of the INM, ratio ~6) and NPC "basket" protein Nup153 (ratio 4.7; Supplemental Table S1). The timing and implications of SINC association with nuclear and nonnuclear host proteins during chlamydial infection are key questions for future work.

Because all four identified SINC-proximal INM proteins are capable of interacting with each other or A- or B-type lamins (Mansharamani and Wilson, 2005; Olins *et al.*, 2010; Berk *et al.*, 2013b; Simon and Wilson, 2013; Shin *et al.*, 2014a), we used GFP pull downs to assess independently potential SINC-GFP association with emerin, lamin B1, or A-type lamins. SINC had no obvious effect on emerin localization in infected cells (Supplemental Figure S4). SINC-GFP specifically coprecipitated native emerin but not native A- or

B-type lamins (Figure 8; $n = 3$). This result supported SINC association with emerin or emerin-containing complexes but did not rule out B-type lamins, which are difficult to solubilize and whose solubility might potentially be influenced by SINC. These results collectively support the conclusion that SINC targets the NE and associates with INM proteins.

DISCUSSION

SINC defines a novel class of bacterial secreted candidate effectors, based on two criteria. First, SINC targets the NE of human cells and associates directly or indirectly with a group of functionally important INM proteins, including two or more LEM-domain proteins. To our knowledge, this targeting of the host NE is unprecedented among bacterial effectors. Second, SINC also exits infected cells and enters presumably uninfected neighbors, where it also concentrates at the NE. The mechanism of SINC intercellular transmission is unknown. There are many potential mechanisms, from packaging within exosomes and release at the cell surface for uptake by neighboring cells (e.g., exploited by *Mycobacterium tuberculosis*; Fleming *et al.*, 2014) to tunneling nanotubes (Marzo *et al.*, 2012). Therefore SINC and its chlamydial orthologues potentially define a novel "nucleomodulin" type of effector (Bierne and Cossart, 2012).

The molecular mechanisms of both novel activities—"INM-tropism" and transfer to the NE of neighboring cells—are major questions for future work. In most other bacteria with T3S systems, effector proteins have an N-terminal secretion "signal," typically followed by a chaperone-binding domain and then a mix of modular, often-unrelated horizontally acquired functional motifs (e.g., soluble N-ethylmaleimide–sensitive factor attachment protein receptor [SNARE], SH3 binding, PDZ binding, NLS, nucleolar localization signal) and domains (e.g., GTPase-activating protein, guanine nucleotide exchange factor, ubiquitin ligase, phosphatase, kinase, AMPylation; Dean, 2011). In stark contrast, our searches using BLAST and PredictProtein showed that SINC, like most chlamydial effectors, has no recognizable motifs or domains (Dehoux *et al.*, 2011; Muschiol *et al.*, 2011; Lutter *et al.*, 2012).

BioID analysis: a powerful new tool to investigate host–pathogen interactions

BioID is a powerful new method that detects close physical proximity between proteins in living cells at specific times chosen by the investigator (Roux *et al.*, 2012; Van Itallie *et al.*, 2013). Our BioID results provided compelling confirmation that SINC associates with the INM, by demonstrating SINC proximity to lamin B1 and specific INM proteins, including emerin, MAN1, LAP1, and LBR, as discussed later. Confirming the BioID results, SINC association with native emerin was demonstrated by GFP pull down from cells. The BioID analysis also revealed SINC proximity to the soluble nuclear import receptor importin-α3, which binds NLS-bearing "cargo" to importin β and to the NPC protein ELYS, consistent with our importazole-based evidence that SINC access to the INM is importin-α/β dependent. Whether SINC influences ELYS, which has a large, unstructured, chromatin-binding domain and is required to recruit the Nup107-160 complex ("Y complex") during nuclear assembly (Franz *et al.*, 2007; Bilokapic and Schwartz, 2013) is unknown. Alternatively, SINC proximity to ELYS and other NPC proteins (e.g., Nup153; Supplemental Table S1) may simply occur during nuclear import.

It must be noted that SINC proximity to these four particular INM proteins was not preordained. The human genome encodes five other LEM-domain proteins (Berk *et al.*, 2013b) and at least 200 other NE membrane proteins (Schirmer *et al.*, 2003; Korfali *et al.*, 2012; de Las Heras *et al.*, 2013), most of which are uncharacterized or limited to specific tissues (de Las Heras *et al.*, 2013). By contrast, the SINC-associated subset of INM proteins—emerin, MAN1, LBR, and LAP1—are widely expressed or ubiquitous in human cells (Zuleger *et al.*, 2013). Of interest, SINC also localized at the NE of *S. cerevisiae*, which lacks lamins and ELYS but expresses other nucleoporins (Field *et al.*, 2014) and proteins orthologous to several SINC-proximal proteins, including LEM-domain proteins (Brachner and Foisner, 2011; Gonzalez *et al.*, 2012) and LBR (Olins *et al.*, 2010). This suggests that SINC targets INM function(s) or pathway(s) that are essential or conserved in a broad spectrum of host tissues, consistent with the broad range of hosts and tissues *C. psittaci* can infect.

The BioID results also revealed SINC proximity to at least 16 additional proteins, opening new directions to understand how host cells are manipulated during *C. psittaci* infection or pathogenesis. These proximal proteins include ER membrane proteins (extended synaptotagmin, LRRC59, SRP receptor, UBXN4) and proteins involved in vesicular trafficking, exocytosis, and calcium homeostasis (VAPA, synaptobrevin) (Garcia *et al.*, 2000; Weir *et al.*, 2001; Quetglas *et al.*, 2002; Yoshihara and Littleton, 2002; De Vos *et al.*, 2012; Morotz *et al.*, 2012). We also identified a mitochondrial protein (mitochondrial antiviral-signaling protein) involved in the innate immune defense against viruses (Jacobs and Coyne, 2013) and vaccinia-related kinase 2 (VRK2), one of two related kinases involved in antiviral defense, suggesting that SINC may target antiviral signaling. On the other hand, VRK1 and VRK2 function in part by inhibiting BAF (*BANF1*; Valbuena *et al.*, 2011; Molitor and Traktman, 2014), the essential DNA- and lamin-binding partner for all LEM-domain proteins (Nichols *et al.*, 2006; Margalit *et al.*, 2007; Suzuki *et al.*, 2010; Berk *et al.*, 2013a). Host proteins identified by proximity to SINC in living cells provide a unique high-throughput resource and platform for future studies of SINC trafficking and function. BioID strategies are readily applicable to other bacterial effectors and host–pathogen interactions (Morriswood *et al.*, 2013). We suggest that BioID will be especially powerful for investigating pathogens like *Chlamydia*, for which relatively few other experimental tools exist.

Modular organization of the SINC polypeptide

Different GFP-fused fragments of SINC showed different subcellular location(s), suggesting that SINC has multiple domains that mediate ER- or INM-specific membrane association (residues 1–164), nuclear import (residues 151–341), or retention within the nucleus (residues 332–502). This modular domain organization is consistent with other characterized T3S effectors from Gram-negative bacteria (Dean, 2011). Our results predict that SINC has at least two separate domains that coordinately interact with NE proteins, because nuclear shape was significantly worse in cells that expressed the N-terminal two-thirds of SINC (residues 1–341; AB-GFP) compared with cells that expressed wild-type SINC-GFP. Candidate NE partners, identified by proximity to BirA-SINC in vivo, include three INM proteins with overlapping functions that can also mutually interact (e.g., emerin, MAN1, LAP1; Berk *et al.*, 2013b; Shin *et al.*, 2014a). One, LAP1, is known to be cleaved by *Chlamydia* protease–like activity factor, a protease released in the cytosol of *C. trachomatis*–infected cells very late in development after lysis of the mature inclusion (Bednar *et al.*, 2011; Snavely *et al.*, 2014). However, the biological effect(s) of the earlier, stable SINC association with the INM in *C. psittaci*–infected cells, its relationship (if any) to SINC transport to neighboring cells, and the effect of SINC transport on *C. psittaci* pathogenesis are major new questions raised by this work. Emerin, MAN1, and LAP1 have overlapping roles important for the heart

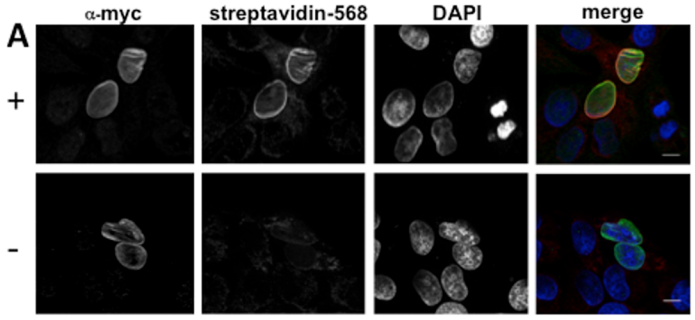

B

	BirA-control total	BirA-SINC total	BirA-SINC specific
BioID1	288	129	30
BioID2	266	146	42

C

REALM	GENE	PROTEIN NAME	FUNCTION	Unique Peptides	Spectral Counts
NE	**LEMD3**	**MAN1**	**INM LEM-domain protein. Antagonizes TGF-β signaling**	**22.5**	**64**
	LBR	**Lamin-B receptor**	**INM protein. Heterochromatin maintenance; binds lamin and Hp1**	**10.5**	**49**
	EMD	**Emerin**	**INM LEM-domain protein; nuclear lamina component**	**8**	**22**
	TOR1AIP1	**Lamina associated protein 1 (LAP1)**	**INM protein. Binds lamins and emerin**	**9**	**25**
	LMNB1	**Lamin-B1**	**Nuclear intermediate filament protein (B-type)**	**4**	**12.5**
	SUN1	SUN domain-containing protein 1	INM component of LINC complexes. Binds KASH-proteins, lamins, emerin	3	8
	LMNA	Prelamin-A/C	Nuclear intermediate filament protein (A-type)	3	5.5
	SUN2	SUN domain-containing protein 2	INM component of LINC complexes. Binds KASH-proteins, lamins, emerin	2	5
NPC/import	**AHCTF1**	**ELYS**	**NPC component. Required for NPC assembly**	**20.5**	**49.5**
	POM121	POM121*	NPC integral membrane protein	5	10
	IMA3	Importin subunit alpha-3*	Nuclear import receptor; links NLS-bearing cargo to importin β (KPNB1)	2	4
	NUP50	Nup50	NPC component	2	2
ER	**ESYT1**	**Extended synaptotagmin**	**Calcium-regulated integral membrane protein; ER structure**	**6**	**12.5**
	UBXN4	**UBX domain-containing protein 4**	**ER-associated protein degradation**	**2.5**	**7.5**
	SRPR	**Signal recognition particle receptor subunit alpha**	**Component of the SRP receptor**	**3.5**	**7.5**
	LRRC59	**Leucine-rich repeat containing protein 59**	**ER/NE protein Binds FGF1; needed for nucl. import of exogenous FGF1**	**3**	**6**
	HACD3	Very-long-chain (3R)-3-hydroxyacyl-[ACP] dehydratase 3	Dehydration step in very long-chain fatty acid (VLCFA) synthesis	2	7
	CAML	Calcium signal-modulating cyclophilin ligand	Receptor for insertion of tail-anchored proteins into ER membrane	2	6
	SRP72	Signal recognition particle receptor subunit SRP72	Targets secretory proteins to the rough ER	2	5
	PREB	Prolactin regulatory element-binding protein	Involved in the formation of COPII vesicles from the ER	2	5
Ves. traffic	**VAPA**	**Vesicle-associated memb. protein-associated protein A**	**May play a role in vesicular trafficking**	**5**	**14**
	YKT6	**Synaptobrevin homolog YKT6**	**SNARE protein; mediates vesicle docking and fusion**	**2**	**4.5**
	VAPB	Vesicle-associated memb. protein-associated protein B/C*	May play a role in vesicular trafficking and calcium homeostasis	4	7
	STIM1	Stromal interaction molecule 1	Calcium sensor at ER	2	6
	SEC24B	Protein transport protein Sec24B*	Component of the COPII coat in ER to Golgi vesicles	2	4
	SYAP1	Synapse-associated protein 1*	Unknown	3	3
	STX5	Syntaxin-5	Mediates ER to Golgi transport	3	3
Cytoskelet.	**WASF2**	**Wiskott-Aldrich syndrome protein family member 2**	**Promotes formation of F-actin**	**4.5**	**12**
	WASF1	Wiskott-Aldrich syndrome protein family member 1	Promotes formation of F-actin	2	6
	WASL	Neural Wiskott-Aldrich syndrome protein	Promotes actin assembly by stimulating Arp2/3 complex	3	6
Membrane	**ABCD3**	**ATP-binding cassette sub-family D member 3**	**Peroxisomal membrane; long-chain fatty acid transport**	**11.5**	**42.5**
	CKAP4	**Cytoskeleton associated protein 4**	**ER/NE membrane protein; links ER to microtubules; also an airway epithelial cell surface receptor for *Pseudomonas aeruginosa***	**6.4**	**16.5**
	AKAP1	**A-kinase anchor protein 1**	**Binds to type I and II regulatory subunits of protein kinase A**	**5**	**14**
	CCD47	**Coiled-coil domain-containing protein 47**	**Unknown**	**5**	**8.5**
	PGRMC2	Memb.-associated progesterone receptor component 2	Receptor for steroids	3	8
	DNM1L	Dynamin-1-like protein	Mitochondrial and peroxisomal division	4	8
	ATPA	ATP synthase subunit alpha	Produces ATP from ADP in presence of proton gradient across memb.	2	5
	GORS2	Golgi reassembly-stacking protein 2	Assembly and stacking of Golgi cisternae	2	5
Signaling	**MAVS**	**Mitochondrial antiviral-signaling protein**	**Required for innate immune defense against viruses.**	**3**	**8.5**
	TACC1	**Transforming acidic coiled-coil-containing protein 1**	**Likely promotes cell division prior to forming differentiated tissues**	**3**	**7**
	DDRGK	**DDRGK domain-containing protein 1**	**Unknown**	**2.5**	**6**
	VRK2	**Serine/threonine-protein kinase VRK2**	**Signaling and innate immunity; phosphorylates BAF (Barrier to autointegration factor; binds LEM-domains and lamins)**	**2.5**	**5**
	SND1	Staphylococcal nuclease domain-containing protein 1	Bridging factor between STAT6 & basal transcription factor	3	8
	ZN207	BUB3-interacting and GLEBS motif-containing protein ZNF207*	Kinetochore-binding protein involved in spindle-assembly checkpoint signaling	3	8
	UB2D3	E3 ubiquitin-protein ligase CBL	Adapter protein, functions as neg. regulator of many signaling pathways	2	4
	UBA1	Ubiquitin-like modifier-activating enzyme 1	Activates ubiquitin by first adenylating its C-terminal G residue with ATP	2	2
RNA-relat.	**TADBP**	**TAR DNA-binding protein 43**	**DNA and RNA-binding protein that regulates transcription and splicing**	**2.5**	**4**
	SR1IP	Protein SREK1IP1*	Possible splicing regulator involved in the control of cellular survival.	2	5
	TDRKH	Tudor and KH domain-containing protein	Primary piRNA biogenesis pathway. Required during spermatogenesis	2	4
Unknown	ANKLE2	Ankyrin repeat and LEM-domain-containing protein 2	Required to dephosphorylate BAF after mitosis; coordinates BAF kinase (VRK1) and phosphatase PP2A	2	7

FIGURE 7: BioID identification of SINC-proximal human proteins. (A) pcDNA3.1-*sinC*–transfected HeLa cells were cultured for 24 h in the continuous presence (+) or absence (–) of 50 μM biotin, fixed with methanol, and stained with DAPI (blue) and myc-specific antibodies (green). Biotinylated proteins were detected using fluorophore-conjugated streptavidin-568 (red). Bar, 10 μm. (B) Number of biotinylated proteins identified by mass spectrometry in two

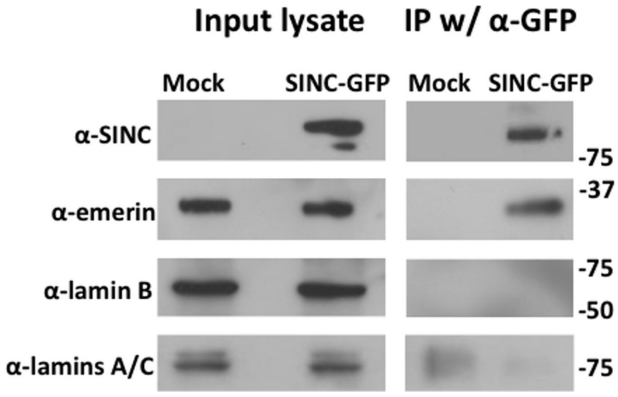

FIGURE 8: Independent confirmation of SINC association with emerin. Immunoblots of input lysates (IPs; 2% loaded in each lane) and GFP pull downs (3% loaded in each lane) from mock-transfected or pCAGGS-*sinC*-GFP–transfected HEK293T cells probed with antibodies specific for SINC (α-SINC), emerin (α-emerin), lamin B (α-lamin B), or lamins A/C (α-lamins A/C). Molecular weight markers (kilodaltons) are shown on the right.

and skeletal muscles (Lu *et al.*, 2011; Berk *et al.*, 2013b; Burke and Stewart, 2013; Shin *et al.*, 2013, 2014b). Although poorly documented, reported complications of psittacosis in humans include pericarditis, endocarditis, myocarditis, and myalgia (Salisch *et al.*, 1996). However, these INM proteins also have diverse roles in NE structure (Fridkin *et al.*, 2009; Simon and Wilson, 2011; Sosa *et al.*, 2013; Berk *et al.*, 2014), cell signaling (Huber *et al.*, 2009; Mendez-Lopez and Worman, 2012), gene regulation (Demmerle *et al.*, 2012; Amendola and van Steensel, 2014), heterochromatin organization (Solovei *et al.*, 2013), cholesterol synthesis (Olins *et al.*, 2010), circadian rhythm (Lin *et al.*, 2014), F-actin regulation in both the cytoplasm and nucleus (Grosse and Vartiainen, 2013; Ho *et al.*, 2013), and autophagy (Park *et al.*, 2009; Deroyer *et al.*, 2014). Many of these pathways are known to be interfered with or exploited by *Chlamydia* species (Carabeo *et al.*, 2003; Pennini *et al.*, 2010; Yasir *et al.*, 2011). Collectively the SINC-proximal proteins provide a blueprint for future studies to map SINC functional domains and understand how and why SINC targets the NE and other host pathways during chlamydial infection.

MATERIALS AND METHODS

Cell culture and chlamydial infection

C. psittaci serovar E strain CAL10 was grown in HeLa 229 cells in 100-mm^2 culture dishes at 37°C with 5% CO_2 in 10 ml of DMEM (Mediatech, Herndon, VA) supplemented with 10% heat-inactivated fetal bovine serum (FBS; Atlanta Biologicals, Lawrenceville, GA), Fungizone (1.25 μg/ml; Life Technologies, Grand Island, NY), and gentamicin (25 μg/ml; Quality Biological, Gaithersburg, MD). To infect cells with chlamydiae, inoculum (1 ml) in SPG (0.25 M sucrose, 10 mM sodium phosphate, 5 mM L-glutamic acid) was added to confluent HeLa cell monolayers to achieve an infection rate of 80%. Monolayers were subsequently rocked for 2 h at 25°C, with hand-rocking every 10–15 min, and finally supplemented with fresh FBS/DMEM.

For inhibitor experiments, HeLa 229 cells grown to confluence on glass coverslips in 24-well plates were infected with *C. psittaci* CAL10 as described. Starting at 24 hpi, cells were treated for 12 h with importazole (22.5 μM) or vehicle DMSO alone. For GFP-pull down experiments, HEK293T cells were used to maximize expression of exogenous polypeptides (see later description).

RT-qPCR

Total RNA was isolated from *C. psittaci* CAL10–infected or mock-infected HeLa 229 cells at 0, 6, 12, 18, 24, 30, 36, 42, or 48 hpi with TRIzol reagent (Life Technologies) per manufacturer's instructions. Total RNA was treated with RNase-free DNase and incubated with or without reverse transcriptase (SuperScript II RT; Life Technologies) and random primers. Primers used in this study are listed in Supplemental Table S2. Primers were designed for *sinC* using the free online tool Primer3 (fokker.wi.mit.edu/primer3/input.htm). Transcripts were quantified by qPCR on 96-well plates using the generated cDNA and IQ SYBR Green Supermix reagent (Bio-Rad, Hercules, CA) by the standard curve method, using 16S rRNA cDNA for normalization (Carrasco *et al.*, 2011). Reactions were performed in duplicate for each time. Expression of target and control genes was quantified from their respective standard curves by conversion of the mean threshold cycle values using iQ5 software (Bio-Rad). Data were normalized as the ratio of *sinC* transcript to 16S rRNA transcript. Statistical analysis was performed with Kruskal–Wallis one-way analysis of variance.

Transfection

PCR products from *C. psittaci* CAL10 genomic DNA encoding full-length SINC or fragments thereof with engineered *Eco*R1 and *Xma*I restriction sites at the ends (primers 070_F/R; Supplemental Table S2) were cloned into the cloning site of mammalian transfection vector pCAGGS-GFP to generate plasmid pCAGGS-*sinC*-GFP and related fragments (Supplemental Table S2). Two endogenous *Eco*R1 sites were removed from the *sinC* nucleotide sequence by introducing silent mutations in two PCRs (primers 070_F/R and Mid_F/R) and used as template for all subsequent cloning experiments. A pCAGGS-*sinC* derivative was obtained using an alternative reverse primer with a stop codon (primer SINC_R2; Supplemental Table S2). PCR products from *C. abortus* and *C. caviae* genomic DNA respectively encoding full-length SINC orthologues CAB063 and CCA_00062 and *C. trachomatis* CT694 were cloned similarly, respectively generating plasmids pCAGGS-*cab063*-GFP (primers 063_F/R), pCAGGS-*cca062*-GFP (primers 062_F/R), and pCAGGS-*ct694*-GFP (primers 694_F/R). One endogenous *Eco*R1 site was removed from the CCA_00062 sequence by introducing a silent mutation in two PCRs (primers 062_F/R and 062Mid_F/R). Unless otherwise indicated, HeLa 229 or HEK293T cells were seeded on glass coverslips in 24-well plates and transfected 24 h later with 500 ng of plasmid (pCAGGS derivatives) in 200 μl of OPTI-MEM and 2 μl of Lipofectamine LTX reagent (Life Technologies), incubated at 37°C, and fixed at indicated times posttransfection for further analysis. To

independent BioID experiments using HEK293 cells that stably expressed BirA-myc (BirA control total) or BirA-myc-SINC (BirA-SINC total) and the number of biotinylated proteins unique to the BirA-SINC pool (BirA-SINC specific). (C) Annotated list of all 50 proteins biotinylated in BirA-myc-SINC–expressing HEK293 cells in one or both BioID experiments. Proteins are categorized according to realm: nuclear envelope (NE); nuclear pore complex/import; endoplasmic reticulum (ER); vesicle traffic; cytoskeleton; membrane; signaling; RNA-related; unknown. Proteins in bold were identified in both BioID 1 and BioID2 (averaged spectral counts and number of unique peptides are indicated). Proteins not in bold were identified only in BioID1 (indicated by asterisk) or BioID2 (no asterisk).

generate stably transfected cells (for BioID; see later description), HEK293 cells growing on 150-mm dishes were transfected using a scaled-up reaction with Lipofectamine LTX reagent. After 48 h, cells were placed under 500 µg/ml G418 selection for 2 wk, with medium changes every 2 d. Stable expression of recombinant polypeptides was assessed by indirect immunofluorescence staining.

Yeast transformation and growth and live imaging

The hemagglutinin tag of the yeast expression vector pRS316/GAL1 (Addgene, Cambridge, MA) was replaced with GFP using a pCAGGS-derived fragment restricted with *Bgl*II and *Xma*I. A PCR product from *C. psittaci* CAL10 genomic DNA encoding full-length SINC with engineered *Sac*II and *Xma*I restriction sites at the ends (primers GAL1_070_F/R) was cloned into the cloning site of pRS316/GAL1, generating pRS316/GAL1-*sinC*-GFP. Yeast strain BY4742 (*MATa his3Δ1 leu2Δ0 met15Δ0 ura3Δ0*) was transformed using the lithium acetate/single-stranded carrier DNA/polyethylene glycol method as described (Gietz and Woods, 2006). Transformants were grown on synthetic complete medium (SC) lacking uracil and supplied with 2% galactose to induce expression. Live transformed yeast cells were imaged on an Axio Imager Z.1 (Zeiss, Jena, Germany) fluorescence microscope.

Generation of α-SINC antibody and immunoblotting

SINC-specific hyperimmune polyclonal antiserum (α-SINC) was generated in two adult guinea pigs (*Cavia porcellus*). Briefly, *sinC* was amplified using primer pair pET30a_070_F/R (Supplemental Table S2) and cloned into pET30a (Novagen, Madison, WI). Recombinant SINC was expressed in BL21 *Escherichia coli* with an N-terminal polyhistidine tag and purified on a 5-ml polypropylene column (Thermo Scientific) with Talon metal affinity resin (Clontech, Mountain View, CA). Guinea pigs were immunized and boosted with purified SINC and hyperimmune serum collected as described previously (Hovis *et al.*, 2013). The antiserum (combined from both immunized animals) was shown to react specifically with a protein band of ~55 kDa, consistent with the predicted molecular weight of SINC in *C. psittaci*–infected cell lysates but not in uninfected and early-cycle lysates (Supplemental Figure S1), and immunoprecipitated a band of ~80 kDa (Figure 8) from pCAGGS-SINC-GFP–transfected cell lysates, consistent with the predicted molecular weight of GFP-SINC.

For immunoblotting, cell lysates were harvested in RIPA buffer containing Complete Mini protease inhibitor cocktail tablets (Roche, Indianapolis, IN), resolved by SDS–PAGE in 12.5% gels (Bio-Rad), and transferred to Amersham Hybond-P polyvinylidene fluoride membranes (GE Healthcare Life Sciences, Little Chalfont, United Kingdom). Membranes were blocked overnight in phosphate-buffered saline (PBS) with 0.1% Tween 20 (PBS-T) and 5% milk, incubated 1 h at 4°C with α-SINC (guinea pig; 1/10,000 dilution; Hovis *et al.*, 2013), α-MOMP (goat; 1/2000; LSBio, Seattle, WA), α-emerin (mouse; 1/2000; Novocastra Laboratories, Newcastle-on-Tyne, United Kingdom), α-lamin A/C (rabbit; Santa Cruz Biotechnology, Santa Cruz, CA), or α-lamin B (mouse; 1/1000; Santa Cruz Biotechnology) primary antibodies, washed three times (5-min each) in PBS-T, detected using horseradish peroxidase–conjugated secondary antibodies specific for guinea pig (Life Technologies), mouse (KPL, Gaithersburg, MD), goat (KPL), or rabbit (GE Healthcare) immunoglobulin G (IgG) in 5% milk PBS-T, and visualized using Supersignal West Femto substrate (Thermo Scientific, Waltham, MA).

Immunofluorescence

Infected HeLa 229 monolayers (at the indicated hours postinfection) or transfected HeLa 229, HEK293, or HEK293T monolayers (at indicated times posttransfection) grown on glass coverslips in 24-well plates were washed with PBS, fixed with methanol or 4% PFA as indicated, and then washed in PBS containing 0.1% Triton X-100 and 1 mg/ml bovine serum albumin (BSA) and stained with 4′,6-diamidino-2-phenylindole (DAPI) in PBS to visualize nuclei and chlamydial inclusions. Monolayers were double stained with α-SINC antibodies and an α–EF-Tu monoclonal antibody kindly provided by Y.-X. Zhang (Boston University, Boston, MA) and visualized using goat anti-mouse IgG conjugated to Alexa Fluor 594 and goat anti-guinea pig IgG conjugated to Alexa Fluor 488 (Life Technologies).

For digitonin permeabilization experiments, cells were fixed in 4% PFA and incubated for 15 min in PBS containing 100 µg/ml digitonin (Sigma-Aldrich, St. Louis, MO). Subsequent wash steps did not contain Triton X-100 or SDS. Cells were stained using rabbit α–lamin A antibodies (PRB-113C; Covance, Princeton NJ) and mouse α-tubulin monoclonal antibody (T5168; Sigma-Aldrich).

For inhibitor experiments, infected monolayers (36 hpi) were washed once with 1× PBS, fixed with methanol, and then stained with α-SINC guinea pig antibodies and Alexa Fluor 594–conjugated goat anti-guinea pig antibodies. All antibodies were used at 1/2000 dilution. Cells were observed on a Zeiss Axio Imager Z.1 fluorescence microscope with the ApoTome.2 module or a Zeiss LSM 510 Meta Confocal Microscope.

Immuno–electron microscopy

At 24 hpi, *C. psittaci*–infected cells were fixed (4% PFA, 0.1M 1,4-piperazinediethanesulfonic acid buffer, pH 7.35), collected, washed, centrifuged, and enrobed in 2.5% low–melting temperature agarose. Agarose blocks (~1 mm^3) were washed and dehydrated using the previously described progressive lowering of temperature technique (Gounon, 2002), infiltrated, and embedded in UNICRYL at –20°C under ultraviolet for times ranging from 24 to 48 h. Ultrathin sections were obtained on a Leica UC6 ultramicrotome (Leica Microsystems, Bannockburn, IL) and collected onto Formvar-coated nickel grids. Immunogold labeling was performed as follows. Inverted grids (section face down) were deposited onto a drop of blocking solution (5% BSA, 0.1% fish gelatin in PBS, pH 7.4) for 30 min, transferred onto a 10-µl droplet of primary antibody diluted in incubation buffer (PBS with 0.2% acetylated BSA, 0.1% fish gelatin) for 1 h at room temperature, washed (5×) in incubation buffer, incubated with 10-nm gold–conjugated secondary antibody for 30–60 min, and washed (5×) again. Grids were then fixed (2% glutaraldehyde in PBS) for 5 min, rinsed with water, contrasted (1% uranyl acetate, 50% methanol), washed again, air dried, and examined on a Tecnai T12 transmission electron microscope (FEI, Hillsboro, OR) at 80 keV. Images were acquired with an AMT digital camera (AMT, Woburn, MA).

Matlab analysis of nuclear circularity

HeLa cells at 24 h postransfection with SINC-GFP (wild type or AB) were fixed with methanol, stained with DAPI, and stained for indirect immunofluorescence with antibodies against GFP or tubulin as the cytoplasmic marker. Images were segmented and analyzed using hTCP, a Matlab script provided by Jacob Sarnecki and Denis Wirtz (Johns Hopkins University, Baltimore, MD; Chen *et al.*, 2013) to measure nuclear circularity. GFP-positive transfectants (n = 300 SINC-GFP wild type; n = 218 SINC AB-GFP) were identified as cells with summed GFP intensities >2 SDs above the mean. Untransfected (GFP-negative) cells numbered 1199 and 1098, respectively. Nuclei in AB-GFP–transfected cells were significantly less circular than nuclei in SINC-GFP–transfected cells ($p < 0.001$; two-tailed t test).

GFP pull-down method

GFP pull down with agarose beads coupled to Alpaca α-GFP antibodies (Chromotek, Planegg, Germany) was done per manufacturer's instructions with some modifications. Briefly, transfected HEK293T cells transiently expressing SINC-GFP (1 × 150–mm dish) and mock-transfected cells were washed thrice with PBS and lysed in 200 µl of lysis buffer (10 mM Tris/HCl, pH 7.5, 150 mM NaCl, 0.5 mM EDTA, 0.5% NP-40). Cells were placed on ice for 30 min with extensive pipetting every 10 min and sonicated once (5–10 s) in a Branson Sonifier 250 (Branson Ultrasonics, Danbury, CT). Lysates were spun at 20,000 × *g* for 10 min, and the supernatants were diluted in wash buffer (10 mM Tris/HCl, pH 7.5, 150 mM NaCl, 0.5 mM EDTA) to 1 ml final volume before incubation with prewashed GFP-Trap-A for 2 h at 4°C. Beads were washed three times with ice-cold wash buffer, and immunocomplexes were disassociated by boiling in SDS–PAGE sample buffer before analysis by immunoblot.

Purification of biotinylated proteins for mass spectrometry

A PCR product from *C. psittaci* CAL10 genomic DNA encoding full-length SINC with engineered terminal *Kpn*I and *Afl*II restriction sites (primers BirA070Fusion_F/R; Supplemental Table S2) was cloned into the multiple cloning site of plasmid pcDNA3.1 mycBioID (kindly provided by Kyle Roux, Sanford Research Center, Sioux Falls, SD), generating pcDNA3.1-*sinC* encoding SINC amino-terminally fused to myc and biotin ligase (BirA-myc-SINC). Transfected HEK293 cells stably expressing either BirA-myc (from pcDNA3.1 mycBioID) or BirA-myc-SINC were incubated for 24 h in complete medium supplemented with 50 µM biotin. Five 150-mm dishes were used for each proteomic analysis. Biotinylated proteins were affinity captured as described (Roux *et al.*, 2012) with slight modifications. Briefly, cells were washed thrice with PBS and lysed in 5 ml of lysis buffer (50 mM Tris, pH 7.4, 500 mM NaCl, 0.4% SDS, 5 mM EDTA, 1 mM dithiothreitol [DTT], 1× complete protease inhibitor [Roche]) and sonicated until the solution was homogeneous. Triton X-100 was added to 2% final concentration. Lysates were then resonicated (5–10 s), supplemented with an equal volume of 50 mM Tris (pH 7.4, 4°C), and sonicated again (5–10 s). Lysates were centrifuged (20 min, 16,000 × *g*), and supernatants were incubated with 500 µl of Dynabeads (MyOne Streptavidin C1; Life Technologies) overnight with rocking. Beads were collected and washed (10 min each, 25°C) sequentially as follows: twice in 1 ml of wash buffer 1 (2% SDS in distilled H_2O), once in wash buffer 2 (0.1% deoxycholate, 1% Triton X-100, 500 mM NaCl, 1 mM EDTA, 50 mM 4-(2-hydroxyethyl)-1-piperazineethanesulfonic acid, pH 7.5), once with wash buffer 3 (250 mM LiCl, 0.5% NP-40, 0.5% deoxycholate, 1 mM EDTA, 10 mM Tris, pH 8.1), and twice with wash buffer 4 (50 mM Tris, pH 7.4, 50 mM NaCl). Finally, beads were washed twice in 50 mM NH_4HCO_3 in preparation for mass spectrometry analysis.

Trypsin digestion and preparation for mass spectrometry

Beads were washed five times (400 µl each) in 25 mM NH_4HCO_3. On-bead tryptic digests were performed by adding 40 µl of sequencing-grade modified trypsin (0.02 µg/µl; Promega, Madison WI) in 25 mM NH_4HCO_3 and incubating for 4 h at 37°C. Tubes containing the beads were placed on a magnetic stand, and supernatants were collected. Beads were washed sequentially with 30 and 10 µl of NH_4HCO_3, saving each supernatant. Supernatants were pooled, and beads were discarded. DL-DTT (8 µl of 200 mM DTT; Sigma-Aldrich) was then added to each solution and incubated 1 h at 37°C. Proteins were alkylated for 45 min at room temperature in the dark with 32 µl of 200 mM iodoacetamide (Sigma-Aldrich) and then quenched by adding 32 µl of 200 mM DTT. Samples were trypsin digested again (0.002 µg/µl, overnight, 37°C) and then acidified by adding 10% trifluoroacetic acid to a final concentration of 1% and desalted on macrospin C18 columns (The Nest Group, Southborough, MA) per manufacturer's instructions. Desalted peptide solutions were lyophilized and resuspended in 15 µl of 5% acetonitrile/0.1% formic acid.

Nano–liquid chromatography–mass spectrometry analysis

Samples were analyzed by electrospray ionization in the positive-ion mode on a hybrid quadrupole-orbitrap mass spectrometer (Q Exactive; Thermo Fisher, San Jose, CA) coupled with a nanoflow LC system (NanoAcquity, Waters Corporation, Milford, MA). A 100-µm inner diameter (i.d.) × 20 mm precolumn was in-house packed with 200-Å, 5-µm C18AQ particles (Michrom BioResources, Auburn, CA). A 75-µm i.d. × 180 mm analytical column was pulled using a P-2000 CO_2 laser puller (Sutter Instruments, Novato, CA) and packed with 100-Å, 5-µm C18AQ particles. Mobile phase A was 0.1% formic acid in water. Mobile phase B was 0.1% formic acid in acetonitrile. For each injection, sample (5 µl) was loaded on the precolumn at 4 µl/min for 10 min in loading buffer (5% acetonitrile, 0.1% formic acid). Peptide separation was performed at 250 nl/min in a 95 min run, in which mobile phase B started at 5%, increased to 35% at 60 min, 80% at 65 min, followed by a 5-min wash at 80% and a 25-min re-equilibration at 5%. Mass spectrometry (MS) data were collected in top-20 data-dependent acquisition experiment with 70K resolution for the full MS scan and 17.5K resolution for higher-energy collisional dissociation (HCD) MS/MS scans. Precursor ions were selected from the full scan *m/z* range of 350–2000 with isolation width of 2 *m/z* and dynamic exclusion of 30 s. HCD fragmentation was performed at normalized collision energy = 35.

Acquired tandem mass spectra were searched against a *Homo sapiens* UniProtKB database using search engine Comet v2014.01. Precursor mass tolerance was set at 10 ppm, and binning tolerance of 0.05 was used on fragment ions. Semi and full trypsin digestion after K or R (except when followed by P) with up to two missed cleavages, carbamidomethylation as static modification, and oxidation of methionine as variable modification were defined as searching parameters. Peptide spectral matches were validated using PeptideProphet and ProteinProphet algorithms. Peptide and protein identifications were filtered at probabilities 0.9 and 0.95, respectively.

ACKNOWLEDGMENTS

We gratefully acknowledge Young Ah Goo of the University of Maryland School of Pharmacy Mass Spectrometry Center (www.pharmacy.umaryland.edu/centers/massspec/) for sample preparation and mass spectrometry analyses, Sarah van Lent for *C. psittaci* cultures used in IEM, Laxmi Yeruva and Roger G. Rank (University of Arkansas for Medical Sciences, Little Rock, AK) for immunizations and collection of α-SINC guinea pig antibodies, and Jacob Sarnecki and Denis Wirtz (Johns Hopkins University, Baltimore, MD) for help with Matlab analysis. This work was supported by Research Grants RO1 GM048646 from the National Institutes of Health, National Institute of General Medical Sciences, to K.L.W. and STI CRC U19 AI084044 from the National Institutes of Health, National Institute of Allergy and Infectious Diseases, to P.M.B. and J.R. S.M. was supported by National Institutes of Health T32 AI007540 and a Graduate Research Assistantship from the University of Maryland, Baltimore, School of Dentistry (Baltimore, MD). The content of this article is solely the responsibility of the authors and does not necessarily represent the official views of the funding institutions.

REFERENCES

Amendola M, van Steensel B (2014). Mechanisms and dynamics of nuclear lamina-genome interactions. Curr Opin Cell Biol 28, 61–68.

Archuleta TL, Du YQ, English CA, Lory S, Lesser C, Ohi MD, Ohi R, Spiller BW (2011). The *Chlamydia* effector chlamydial outer protein N (CopN) sequesters tubulin and prevents microtubule assembly. J Biol Chem 286, 33992–33998.

Arlucea J, Andrade R, Alonso R, Arechaga J (1998). The nuclear basket of the nuclear pore complex is part of a higher-order filamentous network that is related to chromatin. J Struct Biol 124, 51–58.

Bannantine JP, Griffiths RS, Viratyosin W, Brown WJ, Rockey DD (2000). A secondary structure motif predictive of protein localization to the chlamydial inclusion membrane. Cell Microbiol 2, 35–47.

Bednar MM, Jorgensen I, Valdivia RH, McCafferty DG (2011). *Chlamydia* protease-like activity factor (CPAF): characterization of proteolysis activity *in vitro* and development of a nanomolar affinity CPAF zymogen-derived inhibitor. Biochemistry 50, 7441–7443.

Beeckman DSA, Vanrompay DCG (2009). Zoonotic *Chlamydophila psittaci* infections from a clinical perspective. Clin Microbiol Infect 15, 11–17.

Belland RJ, Zhong G, Crane DD, Hogan D, Sturdevant D, Sharma J, Beatty WL, Caldwell HD (2003). Genomic transcriptional profiling of the developmental cycle of *Chlamydia trachomatis*. Proc Natl Acad Sci USA 100, 8478–8483.

Berk JM, Maitra S, Dawdy AW, Shabanowitz J, Hunt DF, Wilson KL (2013a). O-Linked beta-N-acetylglucosamine (O-GlcNAc) regulates emerin binding to barrier to autointegration factor (BAF) in a chromatin- and lamin B-enriched "niche." J Biol Chem 288, 30192–30209.

Berk JM, Simon DN, Jenkins-Houk CR, Westerbeck JW, Gronning-Wang LM, Carlson CR, Wilson KL (2014). The molecular basis of emerin-emerin and emerin-BAF interactions. J Cell Sci 127, 3956–3969.

Berk JM, Tifft KE, Wilson KL (2013b). The nuclear envelope LEM-domain protein emerin. Nucleus 4, 298–314.

Bierne H, Cossart P (2012). When bacteria target the nucleus: the emerging family of nucleomodulins. Cell Microbiol 14, 622–633.

Bilokapic S, Schwartz TU (2013). Structural and functional studies of the 252 kDa nucleoporin ELYS reveal distinct roles for its three tethered domains. Structure 21, 572–580.

Brachner A, Foisner R (2011). Evolvement of LEM proteins as chromatin tethers at the nuclear periphery. Biochem Soc Trans 39, 1735–1741.

Bullock HD, Hower S, Fields KA (2012). Domain analyses reveal that *Chlamydia trachomatis* CT694 protein belongs to the membrane-localized family of type III effector proteins. J Biol Chem 287, 28078–28086.

Burke B, Stewart CL (2013). The nuclear lamins: flexibility in function. Nat Rev Mol Cell Biol 14, 13–24.

Carabeo RA, Mead DJ, Hackstadt T (2003). Golgi-dependent transport of cholesterol to the *Chlamydia trachomatis* inclusion. Proc Natl Acad Sci USA 100, 6771–6776.

Carrasco JA, Tan C, Rank RG, Hsia RC, Bavoil PM (2011). Altered developmental expression of polymorphic membrane proteins in penicillin-stressed *Chlamydia trachomatis*. Cell Microbiol 13, 1014–1025.

Chen WC, Wu PH, Phillip JM, Khatau SB, Choi JM, Dallas MR, Konstantopoulos K, Sun SX, Lee JS, Hodzic D, Wirtz D (2013). Functional interplay between the cell cycle and cell phenotypes. Integr Biol 5, 523–534.

Chu J, Sun R, Wu Z, Liu S, Li D, Zhang Q, Ling Y, Gong Y, Wu R, Wu H, *et al.* (2014). Whole-genome sequences of low-virulence strain CB3 and mild strain CB7 of *Chlamydia psittaci*. Genome Announc 2, e00456–14.

Clifton DR, Fields KA, Grieshaber SS, Dooley CA, Fischer ER, Mead DJ, Carabeo RA, Hackstadt T (2004). A chlamydial type III translocated protein is tyrosine-phosphorylated at the site of entry and associated with recruitment of actin. Proc Natl Acad Sci USA 101, 10166–10171.

Corsaro D, Venditti D (2004). Emerging chlamydial infections. Crit Rev Microbiol 30, 75–106.

da Cunha M, Milho C, Almeida F, Pais SV, Borges V, Mauricio R, Borrego MJ, Gomes JP, Mota LJ (2014). Identification of type III secretion substrates of *Chlamydia trachomatis* using *Yersinia enterocolitica* as a heterologous system. BMC Microbiol 14, 40.

Dean P (2011). Functional domains and motifs of bacterial type III effector proteins and their roles in infection. FEMS Microbiol Rev 35, 1100–1125.

Dehoux P, Flores R, Dauga C, Zhong G, Subtil A (2011). Multi-genome identification and characterization of chlamydiae-specific type III secretion substrates: the Inc proteins. BMC Genomics 12, 109.

de Las Heras JI, Meinke P, Batrakou DG, Srsen V, Zuleger N, Kerr AR, Schirmer EC (2013). Tissue specificity in the nuclear envelope supports its functional complexity. Nucleus 4, 460–477.

Delevoye C, Nilges M, Dautry-Varsat A, Subtil A (2004). Conservation of the biochemical properties of IncA from *Chlamydia trachomatis* and *Chlamydia caviae*: oligomerization of IncA mediates interaction between facing membranes. J Biol Chem 279, 46896–46906.

Demmerle J, Koch AJ, Holaska JM (2012). The nuclear envelope protein emerin binds directly to histone deacetylase 3 (HDAC3) and activates HDAC3 activity. J Biol Chem 287, 22080–22088.

Deroyer C, Renert AF, Merville MP, Fillet M (2014). New role for EMD (emerin), a key inner nuclear membrane protein, as an enhancer of autophagosome formation in the C16-ceramide autophagy pathway. Autophagy 10, 1229–1240.

Derre I, Swiss R, Agaisse H (2011). The lipid transfer protein CERT interacts with the *Chlamydia* inclusion protein IncD and participates to ER-*Chlamydia* inclusion membrane contact sites. PLoS Pathog 7, e1002092.

De Vos KJ, Morotz GM, Stoica R, Tudor EL, Lau KF, Ackerley S, Warley A, Shaw CE, Miller CC (2012). VAPB interacts with the mitochondrial protein PTPIP51 to regulate calcium homeostasis. Hum Mol Genet 21, 1299–1311.

Dumoux M, Clare DK, Saibil HR, Hayward RD (2012). Chlamydiae assemble a pathogen synapse to hijack the host endoplasmic reticulum. Traffic 13, 1612–1627.

Field MC, Koreny L, Rout MP (2014). Enriching the pore: splendid complexity from humble origins. Traffic 15, 141–156.

Fields KA, Fischer ER, Mead DJ, Hackstadt T (2005). Analysis of putative *Chlamydia trachomatis* chaperones Scc2 and Scc3 and their use in the identification of type III secretion substrates. J Bacteriol 187, 6466–6478.

Fields KA, Hackstadt T (2000). Evidence for the secretion of *Chlamydia trachomatis* CopN by a type III secretion mechanism. Mol Microbiol 38, 1048–1060.

Fleming A, Sampey G, Chung MC, Bailey C, van Hoek ML, Kashanchi F, Hakami RM (2014). The carrying pigeons of the cell: exosomes and their role in infectious diseases caused by human pathogens. Pathog Dis 71, 107–118.

Fontoura BM, Dales S, Blobel G, Zhong H (2001). The nucleoporin Nup98 associates with the intranuclear filamentous protein network of TPR. Proc Natl Acad Sci USA 98, 3208–3213.

Franz C, Walczak R, Yavuz S, Santarella R, Gentzel M, Askjaer P, Galy V, Hetzer M, Mattaj IW, Antonin W (2007). MEL-28/ELYS is required for the recruitment of nucleoporins to chromatin and postmitotic nuclear pore complex assembly. EMBO Rep 8, 165–172.

Fridkin A, Penkner A, Jantsch V, Gruenbaum Y (2009). SUN-domain and KASH-domain proteins during development, meiosis and disease. Cell Mol Life Sci 66, 1518–1533.

Garcia RA, Forde CE, Godwin HA (2000). Calcium triggers an intramolecular association of the C2 domains in synaptotagmin. Proc Natl Acad Sci USA 97, 5883–5888.

Gietz RD, Woods RA (2006). Yeast transformation by the LiAc/SS Carrier DNA/PEG method. Methods Mol Biol 313, 107–120.

Giles DK, Wyrick PB (2008). Trafficking of chlamydial antigens to the endoplasmic reticulum of infected epithelial cells. Microbes Infect 10, 1494–1503.

Gong S, Lei L, Chang X, Belland R, Zhong G (2011). *Chlamydia trachomatis* secretion of hypothetical protein CT622 into host cell cytoplasm via a secretion pathway that can be inhibited by the type III secretion system inhibitor compound 1. Microbiology 157, 1134–1144.

Gonzalez Y, Saito A, Sazer S (2012). Fission yeast Lem2 and Man1 perform fundamental functions of the animal cell nuclear lamina. Nucleus 3, 60–76.

Gounon P (2002). Electron microscopy in cellular microbiology: ultrastructural methods for the study of cell surface antigens and pathogenic host—cell interactions. In: Methods in Microbiology, vol. 31, ed. P Sansonetti and A Zychlinsky, New York: Academic Press, 531–557.

Grosse R, Vartiainen MK (2013). To be or not to be assembled: progressing into nuclear actin filaments. Nat Rev Mol Cell Biol 14, 693–697.

Hatch E, Hetzer M (2014). Breaching the nuclear envelope in development and disease. J Cell Biol 205, 133–141.

Hobolt-Pedersen AS, Christiansen G, Timmerman E, Gevaert K, Birkelund S (2009). Identification of *Chlamydia trachomatis* CT621, a protein delivered through the type III secretion system to the host cell cytoplasm and nucleus. FEMS Immunol Med Microbiol 57, 46–58.

Ho CY, Jaalouk DE, Vartiainen MK, Lammerding J (2013). Lamin A/C and emerin regulate MKL1-SRF activity by modulating actin dynamics. Nature 497, 507–511.

Ho TD, Starnbach MN (2005). The *Salmonella enterica* serovar Typhimurium-encoded type III secretion systems can translocate *Chlamydia trachomatis* proteins into the cytosol of host cells. Infect Immun 73, 905–911.

Horn M, Collingro A, Schmitz-Esser S, Beier CL, Purkhold U, Fartmann B, Brandt P, Nyakatura GJ, Droege M, Frishman D, *et al*. (2004). Illuminating the evolutionary history of chlamydiae. Science 304, 728–730.
Hovis KM, Mojica S, McDermott JE, Pedersen L, Simhi C, Rank RG, Myers GS, Ravel J, Hsia RC, Bavoil PM (2013). Genus-optimized strategy for the identification of chlamydial type III secretion substrates. Pathog Dis 69, 213–222.
Hower S, Wolf K, Fields KA (2009). Evidence that CT694 is a novel *Chlamydia trachomatis* T3S substrate capable of functioning during invasion or early cycle development. Mol Microbiol 72, 1423–1437.
Hsia R-C, Pannekoek Y, Ingerowski E, Bavoil PM (1997). Type III secretion genes identify a putative virulence locus of *Chlamydia*. Mol Microbiol 25, 351–359.
Huber MD, Guan T, Gerace L (2009). Overlapping functions of nuclear envelope proteins NET25 (Lem2) and emerin in regulation of extracellular signal-regulated kinase signaling in myoblast differentiation. Mol Cell Biol 29, 5718–5728.
Hybiske K, Stephens RS (2007). Mechanisms of host cell exit by the intracellular bacterium *Chlamydia*. Proc Natl Acad Sci USA 104, 11430–11435.
Ito I, Ishida T, Mishima M, Osawa M, Arita M, Hashimoto T, Kishimoto T (2002). Familial cases of psittacosis: possible person-to-person transmission. Intern Med 41, 580–583.
Jacobs JL, Coyne CB (2013). Mechanisms of MAVS regulation at the mitochondrial membrane. J Mol Biol 425, 5009–5019.
Kaleta EF, Taday EM (2003). Avian host range of *Chlamydophila* spp. based on isolation, antigen detection and serology. Avian Pathol 32, 435–461.
Kim DI, Birendra KC, Zhu W, Motamedchaboki K, Doye V, Roux KJ (2014). Probing nuclear pore complex architecture with proximity-dependent biotinylation. Proc Natl Acad Sci USA 111, E2453–E2461.
Kiseleva E, Drummond SP, Goldberg MW, Rutherford SA, Allen TD, Wilson KL (2004). Actin- and protein-4.1-containing filaments link nuclear pore complexes to subnuclear organelles in *Xenopus* oocyte nuclei. J Cell Sci 117, 2481–2490.
Korfali N, Wilkie GS, Swanson SK, Srsen V, de Las Heras J, Batrakou DG, Malik P, Zuleger N, Kerr AR, Florens L, Schirmer EC (2012). The nuclear envelope proteome differs notably between tissues. Nucleus 3, 552–564.
Kuo CC, Jackson LA, Campbell LA, Grayston JT (1995). *Chlamydia pneumoniae* (TWAR). Clin Microbiol Rev 8, 451–461.
Li ZY, Chen CQ, Chen D, Wu YM, Zhong YM, Zhong GM (2008). Characterization of fifty-putative inclusion membrane proteins encoded in the *Chlamydia trachomatis* genome. Infect Immun 76, 2746–2757.
Lin ST, Zhang L, Lin X, Zhang LC, Garcia VE, Tsai CW, Ptacek L, Fu YH (2014). Nuclear envelope protein MAN1 regulates clock through BMAL1. Elife 3, e02981.
Lu JT, Muchir A, Nagy PL, Worman HJ (2011). LMNA cardiomyopathy: cell biology and genetics meet clinical medicine. Dis Model Mech 4, 562–568.
Lutter EI, Martens C, Hackstadt T (2012). Evolution and conservation of predicted inclusion membrane proteins in chlamydiae. Comp Funct Genomics 2012, 362104.
Lutz-Wohlgroth L, Becker A, Brugnera E, Huat ZL, Zimmermann D, Grimm F, Haessig M, Greub G, Kaps S, Spiess B, *et al*. (2006). *Chlamydiales* in guinea-pigs and their zoonotic potential. J Vet Med A Physiol Pathol Clin Med 53, 185–193.
Mansharamani M, Wilson KL (2005). Direct binding of nuclear membrane protein MAN1 to emerin *in vitro* and two modes of binding to barrier-to-autointegration factor. J Biol Chem 280, 13863–13870.
Margalit A, Brachner A, Gotzmann J, Foisner R, Gruenbaum Y (2007). Barrier-to-autointegration factor–a BAFfling little protein. Trends Cell Biol 17, 202–208.
Marzo L, Gousset K, Zurzolo C (2012). Multifaceted roles of tunneling nanotubes in intercellular communication. Front Physiol 3, 72.
Mendez-Lopez I, Worman HJ (2012). Inner nuclear membrane proteins: impact on human disease. Chromosoma 121, 153–167.
Mojica S, Huot Creasy H, Daugherty S, Read TD, Kim T, Kaltenboeck B, Bavoil P, Myers GS (2011). Genome sequence of the obligate intracellular animal pathogen *Chlamydia pecorum* E58. J Bacteriol 193, 3690.
Molitor TP, Traktman P (2014). Depletion of the protein kinase VRK1 disrupts nuclear envelope morphology and leads to BAF retention on mitotic chromosomes. Mol Biol Cell 25, 891–903.
Moroney JF, Guevara R, Iverson C, Chen FM, Skelton SK, Messmer TO, Plikaytis B, Williams PO, Blake P, Butler JC (1998). Detection of chlamydiosis in a shipment of pet birds, leading to recognition of an outbreak of clinically mild psittacosis in humans. Clin Infect Dis 26, 1425–1429.
Morotz GM, De Vos KJ, Vagnoni A, Ackerley S, Shaw CE, Miller CC (2012). Amyotrophic lateral sclerosis-associated mutant VAPBP56S perturbs calcium homeostasis to disrupt axonal transport of mitochondria. Hum Mol Genet 21, 1979–1988.
Morriswood B, Havlicek K, Demmel L, Yavuz S, Sealey-Cardona M, Vidilaseris K, Anrather D, Kostan J, Djinovic-Carugo K, Roux KJ, Warren G (2013). Novel bilobe components in *Trypanosoma brucei* identified using proximity-dependent biotinylation. Eukaryot Cell 12, 356–367.
Muschiol S, Boncompain G, Vromman F, Dehoux P, Normark S, Henriques-Normark B, Subtil A (2011). Identification of a family of effectors secreted by the type III secretion system that are conserved in pathogenic *Chlamydiae*. Infect Immun 79, 571–580.
Nichols RJ, Wiebe MS, Traktman P (2006). The vaccinia-related kinases phosphorylate the N' terminus of BAF, regulating its interaction with DNA and its retention in the nucleus. Mol Biol Cell 17, 2451–2464.
Olins AL, Rhodes G, Welch DB, Zwerger M, Olins DE (2010). Lamin B receptor: multi-tasking at the nuclear envelope. Nucleus 1, 53–70.
Park YE, Hayashi YK, Bonne G, Arimura T, Noguchi S, Nonaka I, Nishino I (2009). Autophagic degradation of nuclear components in mammalian cells. Autophagy 5, 795–804.
Pennini ME, Perrinet S, Dautry-Varsat A, Subtil A (2010). Histone methylation by NUE, a novel nuclear effector of the intracellular pathogen *Chlamydia trachomatis*. PLoS Pathog 6, e1000995.
Peters J, Wilson DP, Myers G, Timms P, Bavoil PM (2007). Type III secretion a la *Chlamydia*. Trends Microbiol 15, 241–251.
Quetglas S, Iborra C, Sasakawa N, De Haro L, Kumakura K, Sato K, Leveque C, Seagar M (2002). Calmodulin and lipid binding to synaptobrevin regulates calcium-dependent exocytosis. EMBO J 21, 3970–3979.
Rank RG (1994). Animal models for urogenital infections. Methods Enzymol 235, 83–93.
Rank RG, Whittum-Hudson JA (1994). Animal models for ocular infections. Methods Enzymol 235, 69–83.
Read TD, Brunham RC, Shen C, Gill SR, Heidelberg JF, White O, Hickey EK, Peterson J, Utterback T, Berry K, *et al*. (2000). Genome sequences of *Chlamydia trachomatis* MoPn and *Chlamydia pneumoniae* AR39. Nucleic Acids Res 28, 1397–1406.
Read TD, Myers GS, Brunham RC, Nelson WC, Paulsen IT, Heidelberg J, Holtzapple E, Khouri H, Federova NB, Carty HA, *et al*. (2003). Genome sequence of *Chlamydophila caviae* (*Chlamydia psittaci* GPIC): examining the role of niche-specific genes in the evolution of the *Chlamydiaceae*. Nucleic Acids Res 31, 2134–2147.
Rohde G, Straube E, Essig A, Reinhold P, Sachse K (2010). Chlamydial zoonoses. Dtsch Arztebl Int 107, 174–180.
Roux KJ, Kim DI, Raida M, Burke B (2012). A promiscuous biotin ligase fusion protein identifies proximal and interacting proteins in mammalian cells. J Cell Biol 196, 801–810.
Sachse K, Laroucau K, Riege K, Wehner S, Dilcher M, Creasy HH, Weidmann M, Myers G, Vorimore F, Vicari N, *et al*. (2014). Evidence for the existence of two new members of the family *Chlamydiaceae* and proposal of *Chlamydia avium* sp. nov. and *Chlamydia gallinacea* sp. nov. Syst Appl Microbiol 37, 79–88.
Salisch H, von Malottki K, Ryll M, Hinz K-H (1996). Chlamydial infections of poultry and human health. World's Poultry Sci J 52, 279–308.
Samudrala R, Heffron F, McDermott JE (2009). Accurate prediction of secreted substrates and identification of a conserved putative secretion signal for type III secretion systems. PLoS Pathog 5, e1000375.
Satterwhite CL, Gottlieb SL, Romaguera R, Bolan G, Burstein G, Shuler C, Popovic T (2011). CDC grand rounds: Chlamydia prevention: challenges and strategies for reducing disease burden and sequelae. Morbid Mortal Wkly Rep 60, 370–373.
Schirmer EC, Florens L, Guan T, Yates JR3rd, Gerace L (2003). Nuclear membrane proteins with potential disease links found by subtractive proteomics. Science 301, 1380–1382.
Shin JY, Dauer WT, Worman HJ (2014a). Lamina-associated polypeptide 1: protein interactions and tissue-selective functions. Semin Cell Dev Biol 29, 164–168.
Shin JY, Le Dour C, Sera F, Iwata S, Homma S, Joseph LC, Morrow JP, Dauer WT, Worman HJ (2014b). Depletion of lamina-associated polypeptide 1 from cardiomyocytes causes cardiac dysfunction in mice. Nucleus 5, 260–268.
Shin JY, Mendez-Lopez I, Wang Y, Hays AP, Tanji K, Lefkowitch JH, Schulze PC, Worman HJ, Dauer WT (2013). Lamina-associated polypeptide-1 interacts with the muscular dystrophy protein emerin and is essential for skeletal muscle maintenance. Dev Cell 26, 591–603.
Simon DN, Wilson KL (2011). The nucleoskeleton as a genome-associated dynamic "network of networks." Nat Rev Mol Cell Biol 12, 695–708.

Simon DN, Wilson KL (2013). Partners and post-translational modifications of nuclear lamins. Chromosoma 122, 13–31.
Smith KA, Campbell CT, Murphy J, Stobierski MG, Tengelsen LA (2011). Compendium of measures to control *Chlamydophila psittaci* infection among humans (psittacosis) and pet birds (avian chlamydiosis), 2010 National Association of State Public Health Veterinarians (NASPHV). J Exot Pet Med 20, 32–45.
Snavely EA, Kokes M, Dunn JD, Saka HA, Nguyen BD, Bastidas RJ, McCafferty DG, Valdivia RH (2014). Reassessing the role of the secreted protease CPAF in *Chlamydia trachomatis* infection through genetic approaches. Pathog Dis 71, 336–351.
Soderholm JF, Bird SL, Kalab P, Sampathkumar Y, Hasegawa K, Uehara-Bingen M, Weis K, Heald R (2011). Importazole, a small molecule inhibitor of the transport receptor importin-beta. ACS Chem Biol 6, 700–708.
Solovei I, Wang AS, Thanisch K, Schmidt CS, Krebs S, Zwerger M, Cohen TV, Devys D, Foisner R, Peichl L, *et al*. (2013). LBR and lamin A/C sequentially tether peripheral heterochromatin and inversely regulate differentiation. Cell 152, 584–598.
Sosa BA, Kutay U, Schwartz TU (2013). Structural insights into LINC complexes. Curr Opin Struct Biol 23, 285–291.
Stamm WE (1999). *Chlamydia trachomatis* infections: progress and problems. J Infect Dis 179, S380–S383.
Stewardson AJ, Grayson ML (2010). Psittacosis. Infect Dis Clin North Am 24, 7–25.
Subtil A, Delevoye C, Balana ME, Tastevin L, Perrinet S, Dautry-Varsat A (2005). A directed screen for chlamydial proteins secreted by a type III mechanism identifies a translocated protein and numerous other new candidates. Mol Microbiol 56, 1636–1647.
Subtil A, Parsot C, Dautry-Varsat A (2001). Secretion of predicted Inc proteins of *Chlamydia pneumoniae* by a heterologous type III machinery. Mol Microbiol 39, 792–800.
Suchland RJ, Rockey DD, Bannantine JP, Stamm WE (2000). Isolates of *Chlamydia trachomatis* that occupy nonfusogenic inclusions lack IncA, a protein localized to the inclusion membrane. Infect Immun 68, 360–367.
Suzuki Y, Ogawa K, Koyanagi Y, Suzuki Y (2010). Functional disruption of the moloney murine leukemia virus preintegration complex by vaccinia-related kinases. J Biol Chem 285, 24032–24043.
Thomson NR, Yeats C, Bell K, Holden MT, Bentley SD, Livingstone M, Cerdeno-Tarraga AM, Harris B, Doggett J, Ormond D, *et al*. (2005). The *Chlamydophila abortus* genome sequence reveals an array of variable proteins that contribute to interspecies variation. Genome Res 15, 629–640.
Tissera H, Kodiha M, Stochaj U (2010). Nuclear envelopes show cell-type specific sensitivity for the permeabilization with digitonin. Protocol Exchange, doi: 10.1038/protex.2010.211.
Valbuena A, Sanz-Garcia M, Lopez-Sanchez I, Vega FM, Lazo PA (2011). Roles of VRK1 as a new player in the control of biological processes required for cell division. Cell Signal 23, 1267–1272.
Van Itallie CM, Aponte A, Tietgens AJ, Gucek M, Fredriksson K, Anderson JM (2013). The N and C termini of ZO-1 are surrounded by distinct proteins and functional protein networks. J Biol Chem 288, 13775–13788.
Van Itallie CM, Tietgens AJ, Aponte A, Fredriksson K, Fanning AS, Gucek M, Anderson JM (2014). Biotin ligase tagging identifies proteins proximal to E-cadherin, including lipoma preferred partner, a regulator of epithelial cell-cell and cell-substrate adhesion. J Cell Sci 127, 885–895.
Vorimore F, Hsia RC, Huot-Creasy H, Bastian S, Deruyter L, Passet A, Sachse K, Bavoil P, Myers G, Laroucau K (2013). Isolation of a new *Chlamydia* species from the Feral Sacred Ibis (*Threskiornis aethiopicus*): *Chlamydia ibidis*. PLoS One 8, e74823.
Wang Y, Kahane S, Cutcliffe LT, Skilton RJ, Lambden PR, Clarke IN (2011). Development of a transformation system for *Chlamydia trachomatis*: restoration of glycogen biosynthesis by acquisition of a plasmid shuttle vector. PLoS Pathog 7, e1002258.
Weir ML, Xie H, Klip A, Trimble WS (2001). VAP-A binds promiscuously to both v- and tSNAREs. Biochem Biophys Res Commun 286, 616–621.
Wilson DP, Timms P, McElwain DL, Bavoil PM (2006). Type III secretion, contact-dependent model for the intracellular development of *Chlamydia*. Bull Math Biol 68, 161–178.
Wilson DP, Whittum-Hudson JA, Timms P, Bavoil PM (2009). Kinematics of intracellular chlamydiae provide evidence for contact-dependent development. J Bacteriol 191, 5734–5742.
Wilson KL, Berk JM (2010). The nuclear envelope at a glance. J Cell Sci 123, 1973–1978.
Yasir M, Pachikara ND, Bao X, Pan Z, Fan H (2011). Regulation of chlamydial infection by host autophagy and vacuolar ATPase-bearing organelles. Infect Immun 79, 4019–4028.
Yoshihara M, Littleton JT (2002). Synaptotagmin I functions as a calcium sensor to synchronize neurotransmitter release. Neuron 36, 897–908.
Zuleger N, Boyle S, Kelly DA, de las Heras JI, Lazou V, Korfali N, Batrakou DG, Randles KN, Morris GE, Harrison DJ, *et al*. (2013). Specific nuclear envelope transmembrane proteins can promote the location of chromosomes to and from the nuclear periphery. Genome Biol 14, R14.